

## Chapter 6

**DNA & BSA binding and Cytotoxicity  
studies of compartmental ligands  
and complexes**

---

***Chapter 6 DNA & BSA binding and Cytotoxicity studies of compartmental ligands and complexes***

6.1 General Introduction	334
6.2 Interaction of complexes with DNA	336
6.2.1 Important cellular target-DNA	336
6.2.3 Experimental procedures	339
6.2.3.1 UV Absorption studies	340
6.2.3.2 Competitive binding studies with EB using fluorescence spectroscopy	347
6.3 Interaction with proteins - BSA binding studies	356
6.3.1 Serum Albumin: an important biomolecule	356
6.3.2 Materials and instrumentation	357
6.3.3 Experimental section	358
6.3.4 Result and Discussion	371
6.4 Cytotoxicity on Human Hepatoma (HepG2) cell line ( <i>In-cellulo</i> assay)	373
6.4.1 Concept and Principle of MTT assay	373
6.4.2 Materials and instrumentation	374
6.4.2 Experimental section	374
6.4.3 Result and discussion	375
6.5 Conclusion	379
REFERENCES	380

## **6.1 General Introduction**

### ***Cancer: A worldwide epidemic- Research towards its cure***

Cancer (malignant tumour or neoplasm) is the name given to a collection of related diseases. Cancer can start from any part of the human body which is made up of trillions of cells. In normal conditions, human cells grow and divide to form new cells as the body requires them. As they begin to grow old or become damaged, they die, and new cells form which take their place. But in cancer conditions, however, this orderly process breaks down. As the cells become more and more abnormal, old or damaged cells survive instead of dying and new cells form though they are not needed. These extra cells which go on dividing without stopping lead to tumors. Cancerous tumors are malignant, which means they spread into or invade, nearby tissues. As they grow, some cancer cells break off and travel to distant places in the body through blood or lymph system and form new tumors far apart from original tumor (metastasis). Benign tumors don't spread into or invade nearby tissues unlike malignant tumors. Unlike most benign tumors elsewhere in the body, benign brain tumors can be life threatening. There are 100 types of cancer. They are named usually for the organs or tissues where they form. For example, lung cancer starts in the cells of lung, brain cancer starts in the cells of brain and liver cancer starts in the cells of liver.

### ***Worldwide Scenario of Cancer:***

Cancer is a leading cause of death worldwide (nearly 10 million deaths in 2020, or nearly one in six deaths according to World Health Organization. Most common cancers are breast, lung, colon, and rectum and prostate cancers. Around one third deaths from cancer are due to tobacco use, high BMI, alcohol consumption, low fruit or vegetable intake, and lack of physical activity. The most commons in 2020 (in terms of new cases of cancer)<sup>1</sup> were:

- breast (2.26 million cases);
- lung (2.21 million cases);
- colon and rectum (1.93 million cases);
- prostate (1.41 million cases);

- skin (non-melanoma) (1.20 million cases); and
- stomach (1.09 million cases).

The most common causes of cancer death in 2020<sup>1</sup> were:

- lung (1.80 million deaths);
- colon and rectum (916 000 deaths);
- liver (830 000 deaths);
- stomach (769 000 deaths); and
- breast (685 000 deaths).

Each year, approximately 400 000 children develop cancer. The most common cancers vary between countries. Cervical cancer is the most common in 23 countries.

***Development of metal complexes as artificial nucleases:***

The metal complexes as pharmaceuticals have gained access over traditional drugs containing organic moieties, due to their potential use as regulators of gene expression and tools of molecular biology. The major intracellular target of anticancer metallodrugs is DNA; therefore, metal complexes that can bind to specific nucleotides of DNA are of interest. Studies of metal complexes, which react at specific sites along a DNA strand, provide routes toward the rational development of chemotherapeutic agents, sensitive chemical probes for DNA structure in solution and tools for the molecular biologist to dissect genetic systems. In this regard, transition metal complexes are outstanding as artificial nucleases for DNA due to their diverse ability to recognize and react selectively with individual target sites. At the same time, the presence of redox active transition metal ions can further help oxidative cleavage of impaired DNA. This has stimulated considerable interest in a search for new metal complexes as modern therapeutics, diagnostic and radiopharmaceutical agents. The coordination chemistry of bioactive molecules becomes important for their biological applications because the bioactive molecules choose and interact with the bioactive sites mainly through the supramolecular interactions and then the metal ions can further exert their effect through an associated redox, by inducing polarization and/or through template effect. Complexes of metal ions, especially, the biologically essential metal ions like copper

have been reported to have good biological activities like DNA binding<sup>2-6</sup>, BSA binding<sup>7-12</sup> and cytotoxicity.<sup>13-21</sup>

***Brief about the investigations in the present work:***

The work presented in this chapter envisages the anticancer property of a few selected binuclear copper(II) complexes synthesized as part of this thesis. The as-synthesized copper(II) complexes described in previous chapters have been investigated upon for their anticancer properties in a stepwise manner starting from the preliminary *in vitro* evaluations on interactions with basic biomolecules like DNA and Bovine serum albumin which were carried out outside cellular environment employing spectroscopic titration method within cuvette. The result so obtained in these studies further prompted us to indulge into *in cellulo* studies comprising of the basic cytotoxicity evaluation on Human Hepatoma (HepG2) cancer cell lines and calculating corresponding IC<sub>50</sub> values of few selected binuclear copper(II) complexes. These have been discussed in detail in the current chapter.

## **6.2 Interaction of complexes with DNA**

### **6.2.1 Important cellular target-DNA**

The primary carrier of all genetic information is biopolymer DNA. DNA provides the “*master genetic blueprint*” for the construction of each protein required by individual cells through RNA mediated processes of transcription and translation. Small molecules and /or proteins that bind to nucleic acids in site-specific ways initiate, regulate, and terminate all these processes. Such synthetic molecules that interact with nucleic acids or modulate their function have found a variety of uses as biophysical and therapeutic agents.<sup>22</sup> For the design of DNA-interactive systems, coordination complexes are ideal templates in many ways, and intensive research has been carried out for the study of interaction of these structurally complex three-dimensional architectures with DNA. In addition to various binding modes, metal complexes coordinate directly to DNA Lewis base sites where they undergo redox reactions with DNA or generate reactive oxygen species. The ability of metal complexes to bind and cleave DNA which interfere with the essential cellular processes of transcription and translation means that these systems could also be developed as potential therapeutics. The principal interactions generally used to target DNA are briefly outlined below:

**Different modes of drug-DNA interactions:**

The structure and chemical composition of DNA leads to several mechanisms by which molecular substrates can bind to DNA and such interactions can be irreversible (covalent binding) or reversible (non-covalent binding). (**Figure 6.2.1.1**)

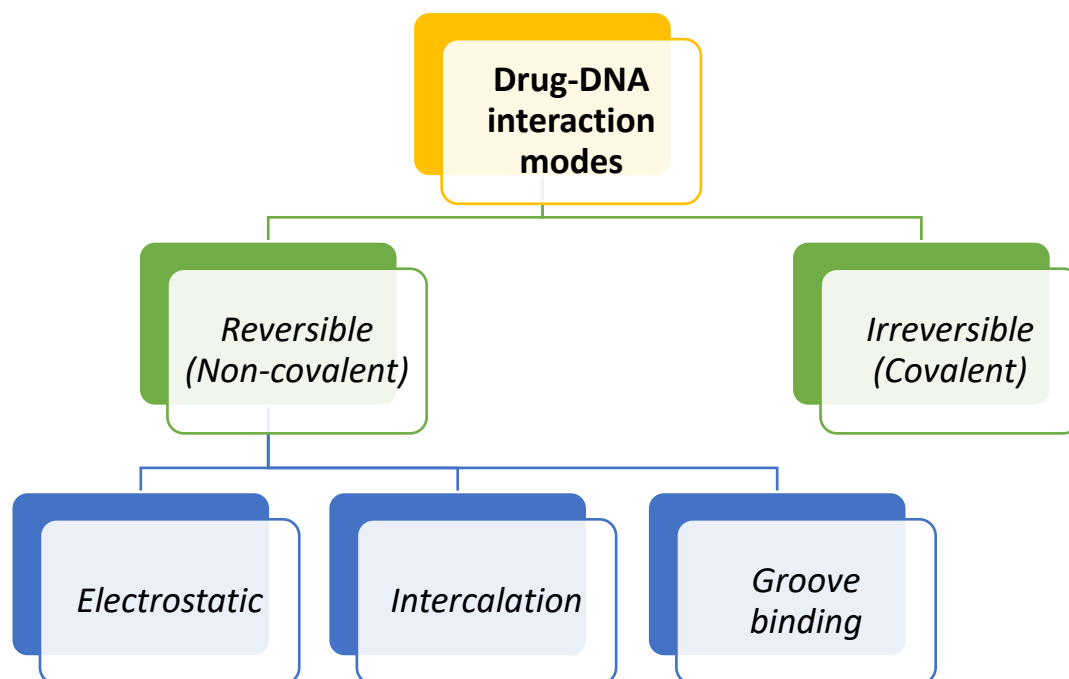


*Figure 6.2.1.1 Different modes of Drug-DNA interactions*

*Irreversible (covalent) binding to DNA*

Covalent bonds are formed between the molecules and phosphodiester backbone, sugar residues or base of the DNA molecule. This is the most common method of DNA interaction for known clinically used anticancer drugs. Cisplatin and its derivatives offers the paradigm of this approach: it interact with DNA through coordination bonds formed between the Pt(II) centers and available nitrogen atoms on nucleotides, commonly N7 atoms on adjacent purine bases (**Figure 6.2.1.2A**). Based on the success of cisplatin and its derivatives, including copper(II)-based systems, have been designed to display a similar function.

*Reversible (non-covalent) binding to DNA*

This mode of binding is an attraction for researchers. These systems exploit several reversible binding motifs:

- I. Electrostatic interactions:** The cationic molecules can associate with negative charge of DNA. Naturally occurring polyamines such as spermine bind to DNA through such interactions. Majority of coordination compounds are charged, so electrostatic interactions contribute to the binding affinity of complexes to DNA, which predominantly recognize DNA through binding modes described ahead.
- II. Intercalation** (Figure 6.2.1.2B): Mostly all metal complexes reversibly interact with DNA by metallo-intercalators. It occurs when planar aromatic compounds are inserted between adjacent base pairs in DNA double helix. It involves  $\pi$  system overlap between DNA bases and the intercalated molecule, as well as van der Waals, hydrophobic and electrostatic interactions which has effect of unwinding and lengthening of DNA double helix.
- III. Groove binding** (Figure 6.2.1.2C): This is another mode of reversible binding to DNA by association within the minor or major grooves that run down the double helix. Molecules approach within van der Waals contact distances of the groove walls and then occupy DNA grooves. Classical groove binders are usually cationic and composed of aromatic rings by bonds with torsional freedom, so they are able to twist and become iso-helical with DNA groove.

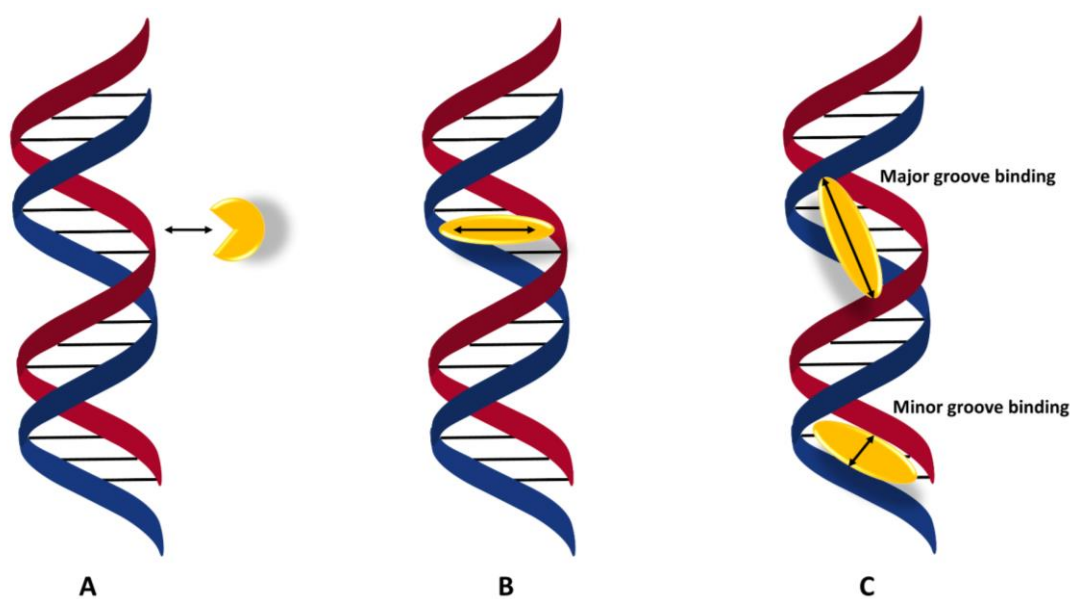


**Figure 6.2.1.2** Schematic representation of the three major modes of drug-DNA interactions: (A) Covalent binding, (B) Intercalation binding and (C) Groove binding.

### **6.2.2 Materials and Instrumentation**

ct-DNA, tris-buffer, ethidium bromide, tris buffer HCl were procured from SRL for the DNA binding studies. All these chemicals were used without any further purification. Conc HCl used for adjusting the pH = 7.5 while preparing the buffer and DMSO used to prepare the stock solutions were of analytical grade and were purchased from Spectrochem.

The mode and DNA propensity of the synthesized complexes were analyzed by different spectral techniques. All experiments involving interaction of complexes with ct-DNA were performed in tris(hydroxymethyl)-aminomethane-HCl (15 mM)/NaCl (150 mM) buffer (pH adjusted to 7.5 with conc. HCl). DNA stock solution was prepared by dissolving a strand of ct-DNA in double distilled water and kept at 4°C for no longer than a week. The stock solution of ct DNA gave a ratio of UV absorbance at 260nm and 280nm ( $A_{260}/A_{280} \leq 1.90$ ), indicating that DNA was sufficiently free of protein contamination.<sup>23</sup> The concentration of calf thymus-DNA (solution prepared in TRIS-HCl/NaCl buffer) was acquired from absorption intensity observed at 260 nm using molar extinction coefficient value of  $6600 \text{ M}^{-1}\text{cm}^{-1}$ .<sup>24</sup> The DNA-binding experiments were performed at  $\sim 30.0^\circ\text{C}$ . Stock solution of EB (ethidium bromide) was prepared in double distilled water with a concentration of  $10^{-3} \text{ M}$ .

#### **UV-vis spectroscopy**

UV-vis spectrophotometer was used to carry out studies of metal complexes and ligands. The spectrum was recorded using Perkin Elmer Lambda 35 dual beam UV-vis Spectrophotometer.

#### **Fluorescence spectroscopy**

Fluorescence spectra was recorded in solution phase on JASCO FP-6300 fluorescence spectrophotometer.

The data generated from titration experiments was analyzed and plotted with the help of software Origin 2019b.

### **6.2.3 Experimental procedures**

To target cellular DNA by a compound, simple *in-vitro* experiments can be performed to readily determine whether the compound physically interacts with

DNA. These assays can be powerful tools to determine the mechanism of previously discovered molecules and will be a crucial discovery of the next generation of DNA anticancer drugs. Two such techniques: (a) UV-Vis absorption studies and (b) Competitive binding studies with EB using fluorescence spectroscopy; have been exploited the most for studying DNA binding with synthesized molecules which are spectroscopy based titration methods.

#### 6.2.3.1 UV Absorption studies

Absorption spectroscopy has been used to test the presence of ground state interactions between biological macromolecule DNA and compounds under study. It helps to investigate the binding efficiency of the complexes to DNA since the observed spectral changes may give evidence of the existing interactions mode.<sup>25</sup> These interactions may be due to ligand or metal centered transitions of the compounds. DNA binds with compounds *via* non-intercalative binding modes, such as electrostatic forces, van der Waals interactions, dative bonds, H-bonds and hydrophobic interactions which results in increase in absorption intensity (hyperchromism) upon increasing concentration of ct-DNA. It is likely that the amine or hydroxyl containing group forms H-bonds with N-3 adenine or O-2 of thymine in DNA which results in hyperchromism since DNA possesses several H-bonding sites which are accessible both in minor and major grooves. Electrostatic interactions occurs between positively charged groups of the compound and negatively charged phosphate backbone at the periphery of the double helix ct-DNA which leads to hyperchromism effect.<sup>26</sup> In intercalative mode, there is stacking interaction between the ligand and a DNA base pair. It involves the interaction of  $\pi^*$  orbital of the intercalating ligand binds with  $\pi$  orbital of DNA base pairs which leads to decrease in  $\pi \rightarrow \pi^*$  transition energy and results in bathochromism. On the other hand, the coupling of  $\pi$  orbital to an orbital partially filled by electrons decreases the transitional probabilities and results into hypochromism. Thus, as a general observation, the binding of an intercalative molecule to DNA is accompanied by hypochromism and significant red shift (bathochromism) in the absorption spectra due to a very strong interaction of aromatic chromophore of the ligand and DNA base pairs<sup>19</sup> and the shift in the wavelength is indicative of the strength of the interaction.

The interactions of compounds (under study) with ct-DNA have been studied with UV spectroscopy in order to investigate the possible mode of binding with ct-DNA and to evaluate the extent of interaction through the value of binding constant ( $K_b$ ). These studies were performed with constant concentrations of compounds while varying the concentration of ct-DNA. Stock solutions of compounds were diluted with tris buffer to get desired concentrations. Equal increments of ct-DNA were added in different ratios to both sample and reference cell to eliminate the absorbance of ct-DNA itself. The titration graph so generated has been representatively shown for all compounds in **Figure 6.2.4.1A-D**. The ratio of the [DNA]:[compound] has been mentioned in each of the cases as legends, in the graphs.

The magnitude of binding strength to ct-DNA may be determined through the calculation of binding constant  $K_b$  which is obtained by monitoring the changes in the absorbance of the compounds with increasing concentrations of ct-DNA. The data obtained from the absorption titration experiment is fitted in **eq. 6.1** wherein  $K_b$  is given by ratio of slope to the  $y$  intercept in plots of  $[DNA]/(\epsilon_A - \epsilon_F)$  versus  $[DNA]$  according to Mehan's equation<sup>27</sup> (**eq. 6.1**)

$$[DNA]/(\epsilon_A - \epsilon_F) = [DNA]/(\epsilon_b - \epsilon_F) + 1/K_b(\epsilon_b - \epsilon_F) \quad (6.1)$$

where  $[DNA]$  = concentration of DNA in base pairs,  $\epsilon_A = A_{\text{obsd}}/[\text{compound}]$ ,  $\epsilon_F$  = extinction coefficient for unbound compound and  $\epsilon_b$  = extinction coefficient for compound in fully bound form. The  $K_b$  plots for all synthesized ligands and their corresponding complexes have been shown in **figure 6.2.4.2**. The  $K_b$  values obtained from the plots have been tabulated and discussed with significance to their structures in **section 6.2.4**.

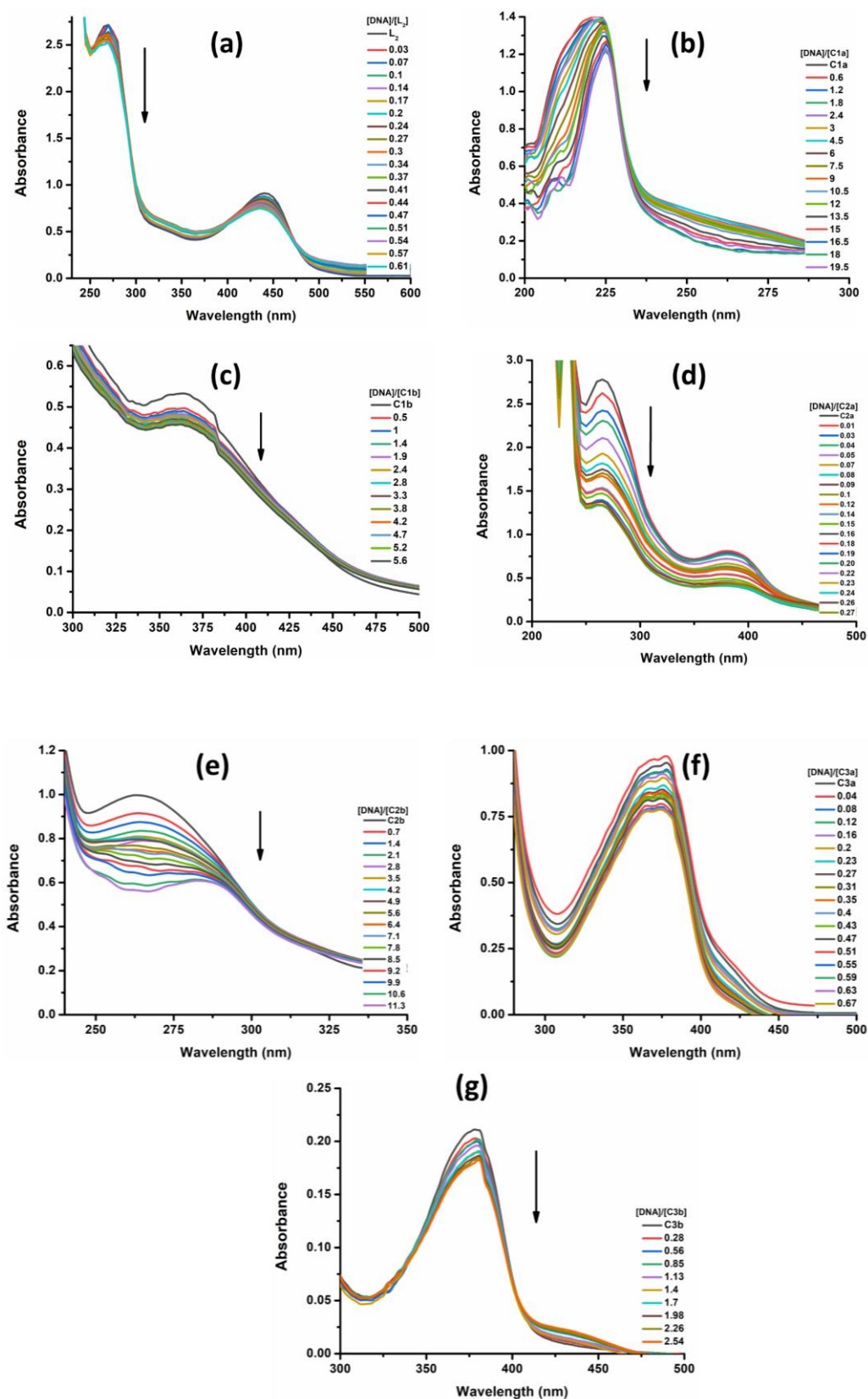


**Figure 6.2.4.1A** Absorption spectra for the spectrophotometric titration of (a)  $L^2$  (b) C1a (c) C1b (d) C2a (e) C2b (f) C3a and (g) C3b in absence and presence of ct-DNA at 30°C in 15 mM Tris-HCl/150 mM NaCl buffer (pH=7.5). The downward arrow shows a decrease in absorption intensity with increasing DNA concentrations

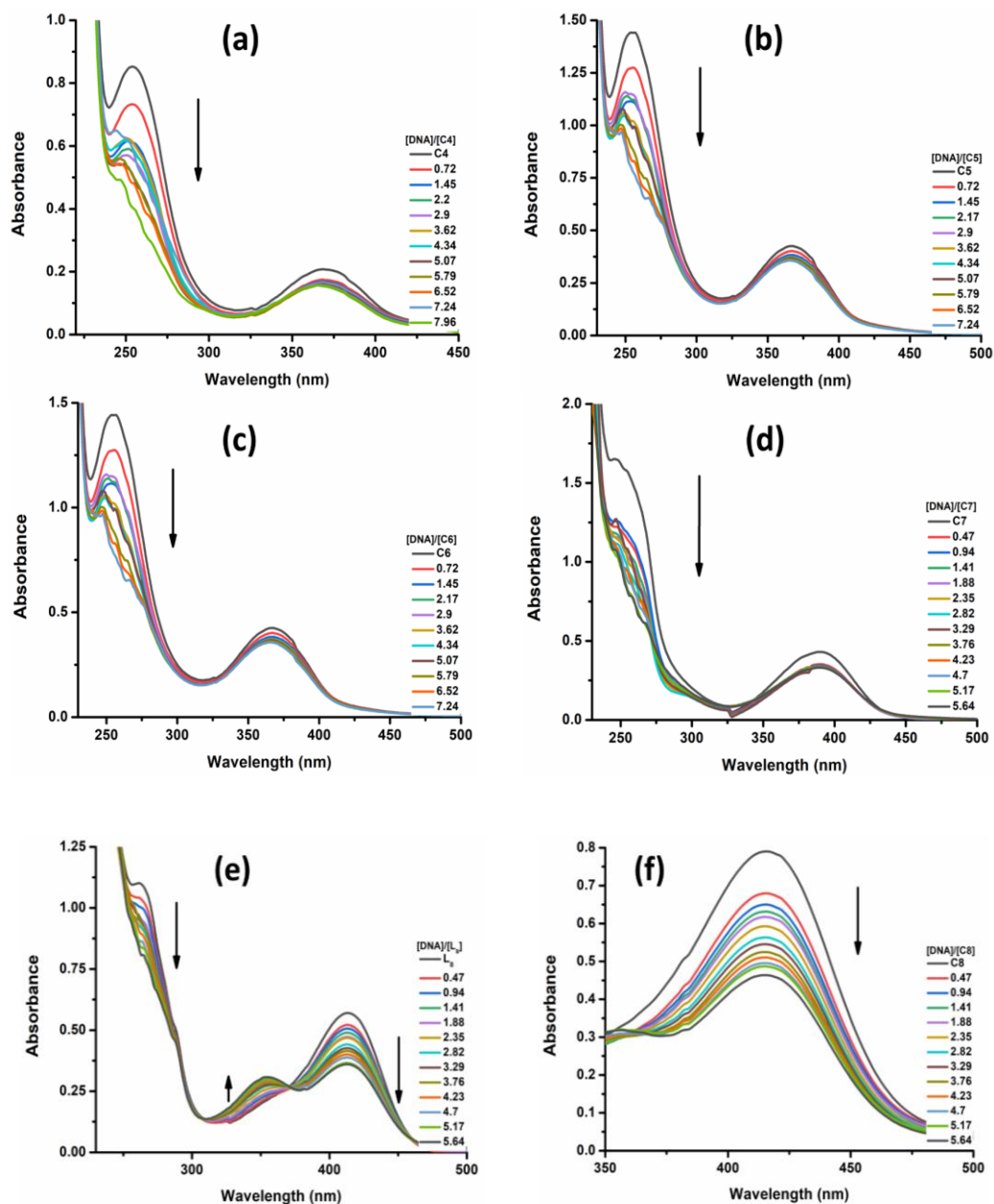


**Figure 6.2.4.1B** Absorption spectra for the spectrophotometric titration of (a) C4 (b) C5 (c) C6 (d) C7 (e) L<sup>8</sup> and (f) C8 in absence and presence of ct-DNA at 30°C in 15 mM Tris-HCl/150 mM NaCl buffer (pH=7.5). The downward arrow shows a decrease in absorption intensity with increasing DNA concentrations

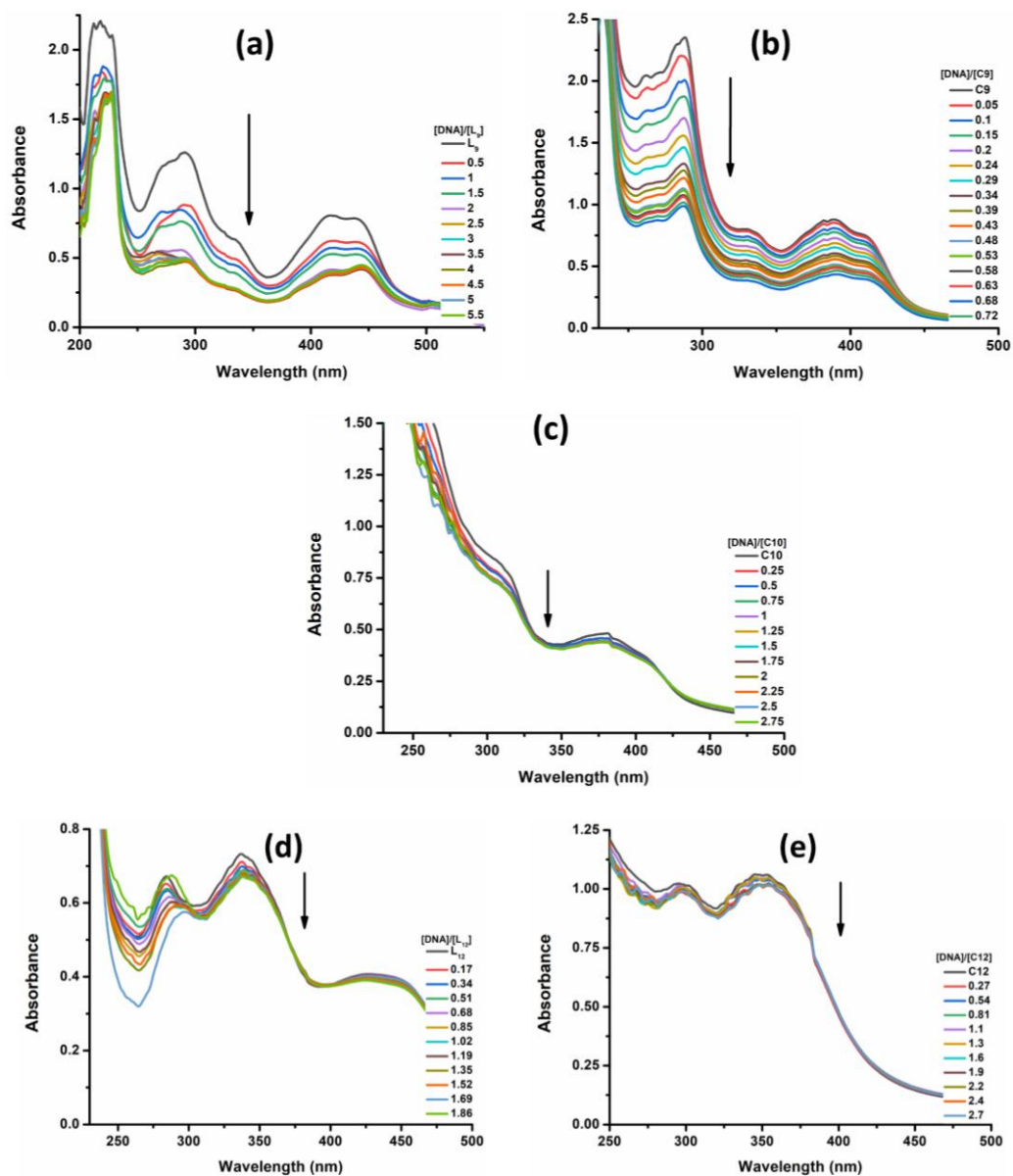


**Figure 6.2.4.1C** Absorption spectra for the spectrophotometric titration of (a)  $L^9$  (b) C9 (c) C10 (d)  $L^{12}$  and (e) C12 in absence and presence of ct-DNA at 30°C in 15 mM Tris-HCl/150 mM NaCl buffer (pH=7.5). The downward arrow shows a decrease in absorption intensity with increasing DNA concentrations

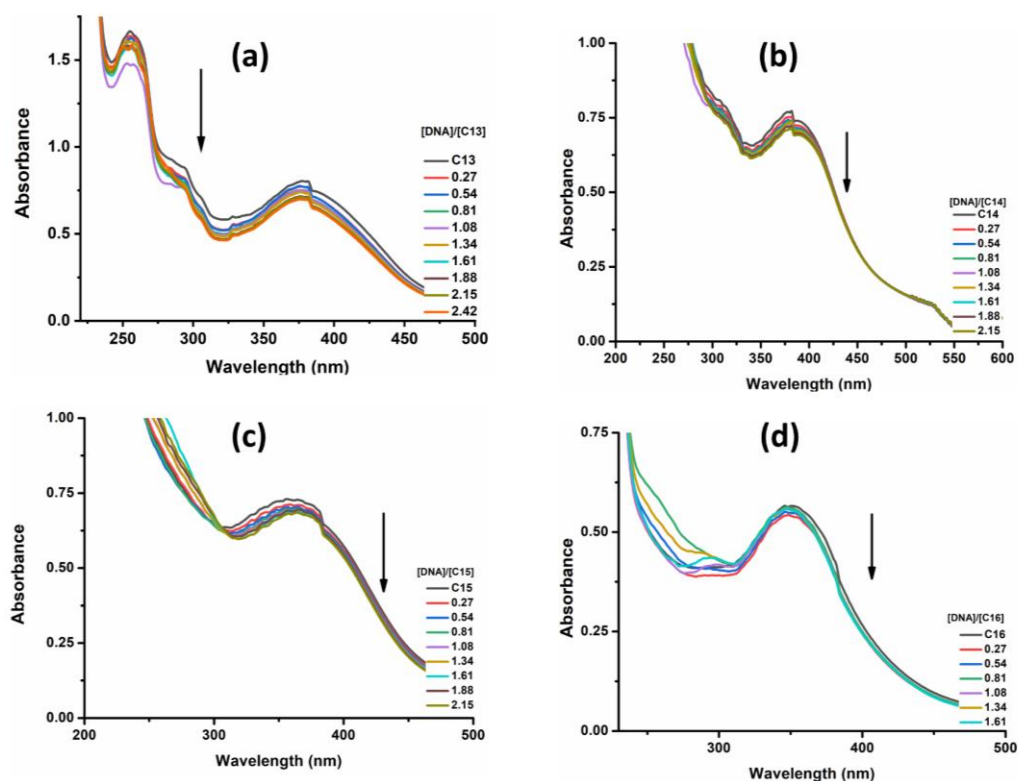


**Figure 6.2.4.1D** Absorption spectra for the spectrophotometric titration of (a) C13 (b) C14 (c) C15 and (d) C16 in absence and presence of ct-DNA at 30°C in 15 mM Tris-HCl/150 mM NaCl buffer (pH=7.5). The downward arrow shows a decrease in absorption intensity with increasing DNA concentrations

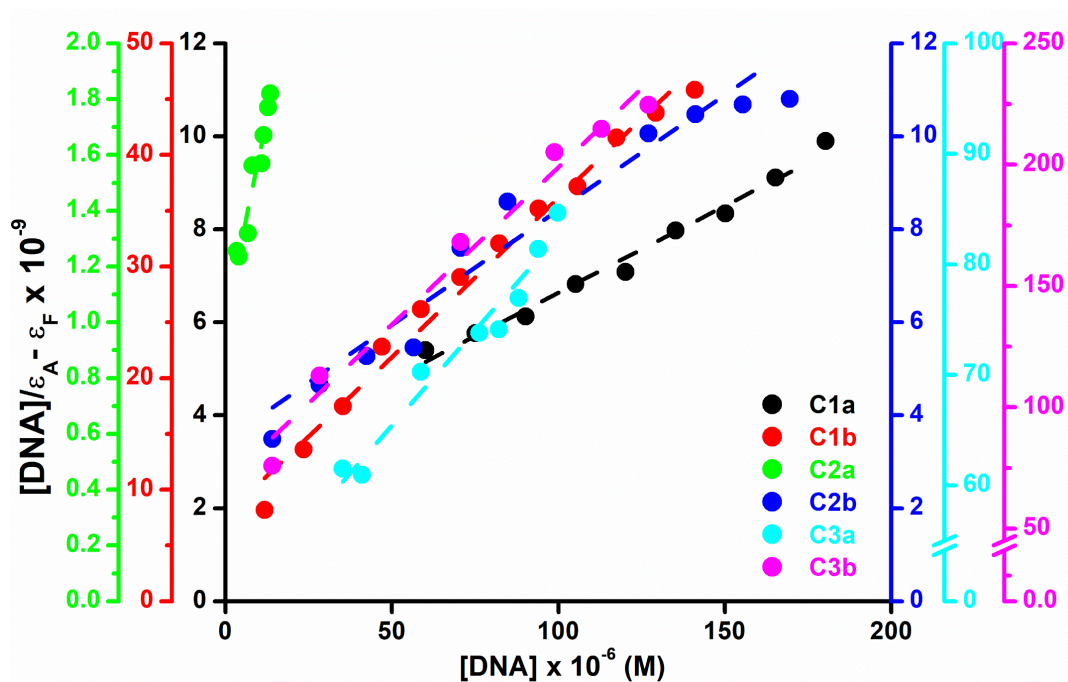


**Figure 6.2.4.2A** Plots of  $[DNA]/(\epsilon_A - \epsilon_F)$  vs  $[DNA]$  for complexes C1a-C3a and C1b-C3b

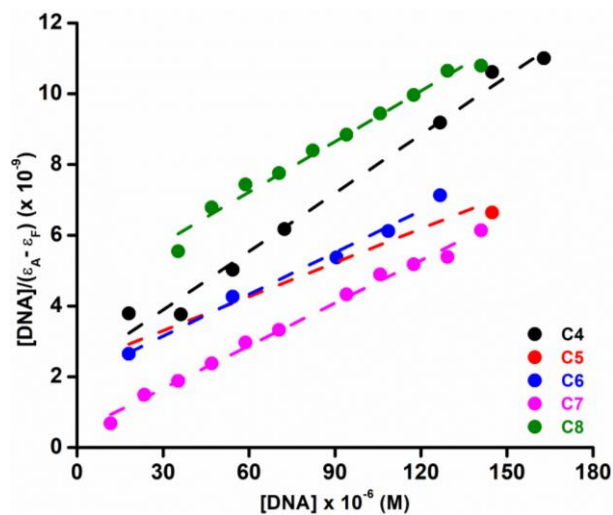


Figure 6.2.4.2B Plots of  $[DNA]/(\epsilon_A - \epsilon_F)$  vs  $[DNA]$  for complexes C4-C8

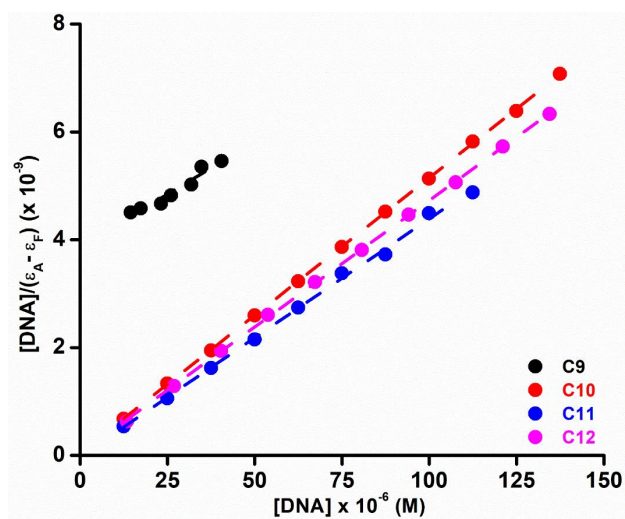


Figure 6.2.4.2C Plots of  $[DNA]/(\epsilon_A - \epsilon_F)$  vs  $[DNA]$  for complexes C9, C10 and C12

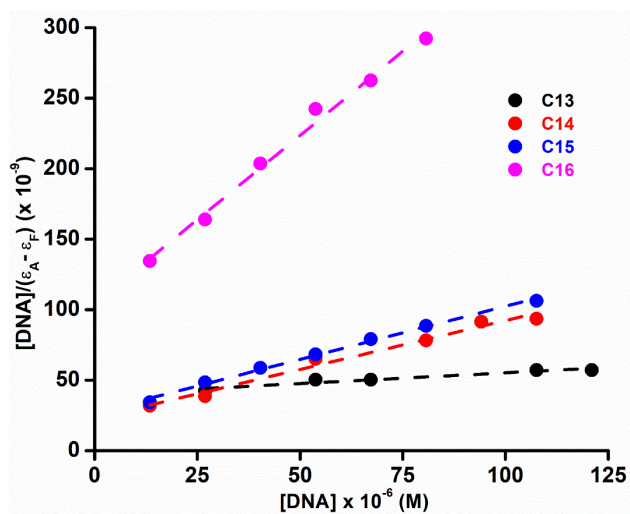


Figure 6.2.4.2D Plots of  $[DNA]/(\epsilon_A - \epsilon_F)$  vs  $[DNA]$  for complexes C13-C16

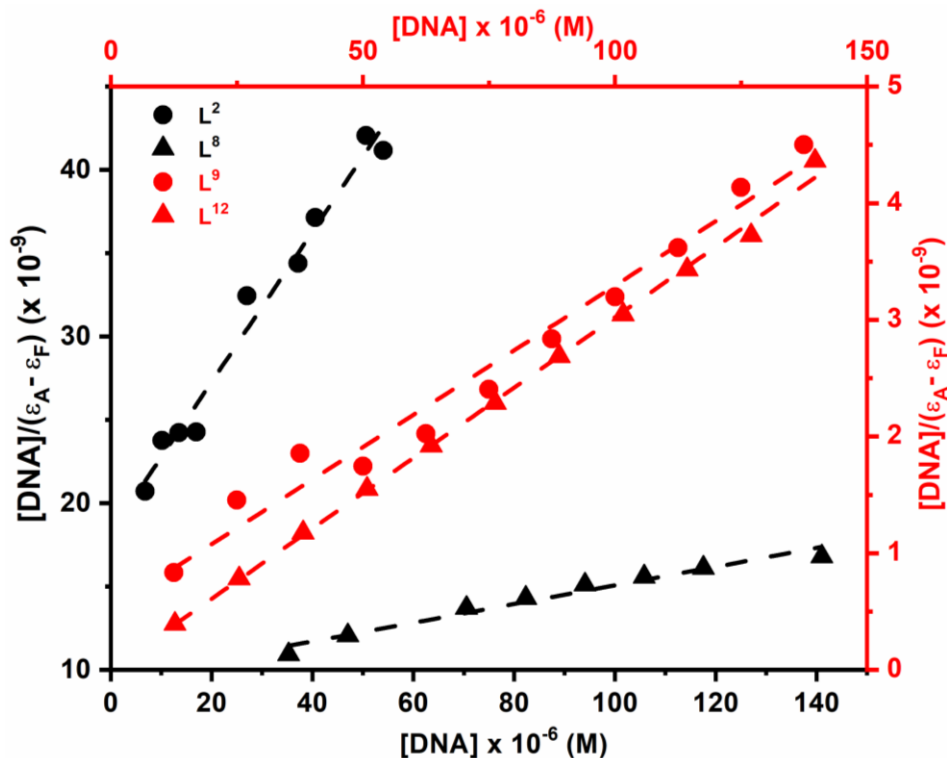


Figure 6.2.4.2E Plots of  $[DNA]/(\epsilon_A - \epsilon_F)$  vs  $[DNA]$  for ligands ( $L^2$ ,  $L^8$ ,  $L^9$  and  $L^{12}$ )

### 6.2.3.2 Competitive binding studies with EB using fluorescence spectroscopy

A competitive binding study has been employed using fluorescence spectroscopy in order to examine the ability of a compounds to displace EB from its DNA-EB complex.<sup>18</sup> Ethidium Bromide (EB = 3,8-diamino-5-ethyl-6-phenyl-phenanthridinium bromide) a phenanthridine fluorescent dye is a typical indicator of intercalation, forming soluble complexes with nucleic acids and emitting intense fluorescence in the presence of DNA due to the intercalation of the planar phenanthridine ring between adjacent base pairs on the double helix.<sup>28,29</sup> Addition of a second molecule (compound under study), which may replace EB from the DNA-EB complex results in a decrease of the DNA-induced EB emission due to displacement of EB from the intercalation sites of DNA.<sup>30</sup> Thus the displacement of EB (quantified by fluorescence) by the addition of a compound is suggestive of an intercalative binding.<sup>31,32</sup>

To examine whether compounds can displace EB from DNA-EB complex, the competitive binding study of each compound with DNA-EB has been investigated with fluorescence spectroscopy. For emission studies, DNA-EB complex was prepared by adding solution containing DNA and 33.33 $\mu$ M EB in TRIS-HCl/NaCl

buffer in a cuvette. The titration experiment was carried out by keeping DNA-EB complex concentration constant and varying the compound concentration by adding an increasing amount of solution one by one into it. The variation in the fluorescence emission spectra of the DNA-EB complex due to addition of each aliquot of the compound was recorded at RT (303 K). The influence of complexes on DNA-EB was recorded at 610nm ( $\lambda_{\text{ex}} = 546$  nm, bandwidth=2.5nm for both excitation and emission) after addition of different concentrations of the compound at different ratios. The titration curve so generated and the ratio of the [quencher]:[DNA] has been mentioned in each of the cases as legends, in the graphs represented in the **figure 6.2.4.3A-D**. The relative binding of the complexes to ct-DNA was determined by calculating the quenching constant ( $K_{SV}$ ) from the slope of the straight lines obtained from Stern-Volmer equation (**eq 6.2**)<sup>33</sup>:

$$I_0/I = 1 + K_{SV}[Q] \quad (6.2)$$

where  $I_0$  and  $I$  are the emission intensities in the absence and the presence of the quencher (Q=compound) respectively,  $[Q]$  is the concentration of the quencher and  $K_{SV}$  is the Stern-Volmer constant which can be obtained from slope of the plot of  $I_0/I$  versus  $[Q]$  and is often used to evaluate the quenching efficiency of each compound.

The  $K_{SV}$  plots for all synthesized ligands and their corresponding Cu(II) complexes have been shown in **figure 6.2.4.4**. The  $K_{SV}$  values obtained from these plots have been tabulated (**Table 6.2.4.1**) and discussed in **section 6.2.4**.

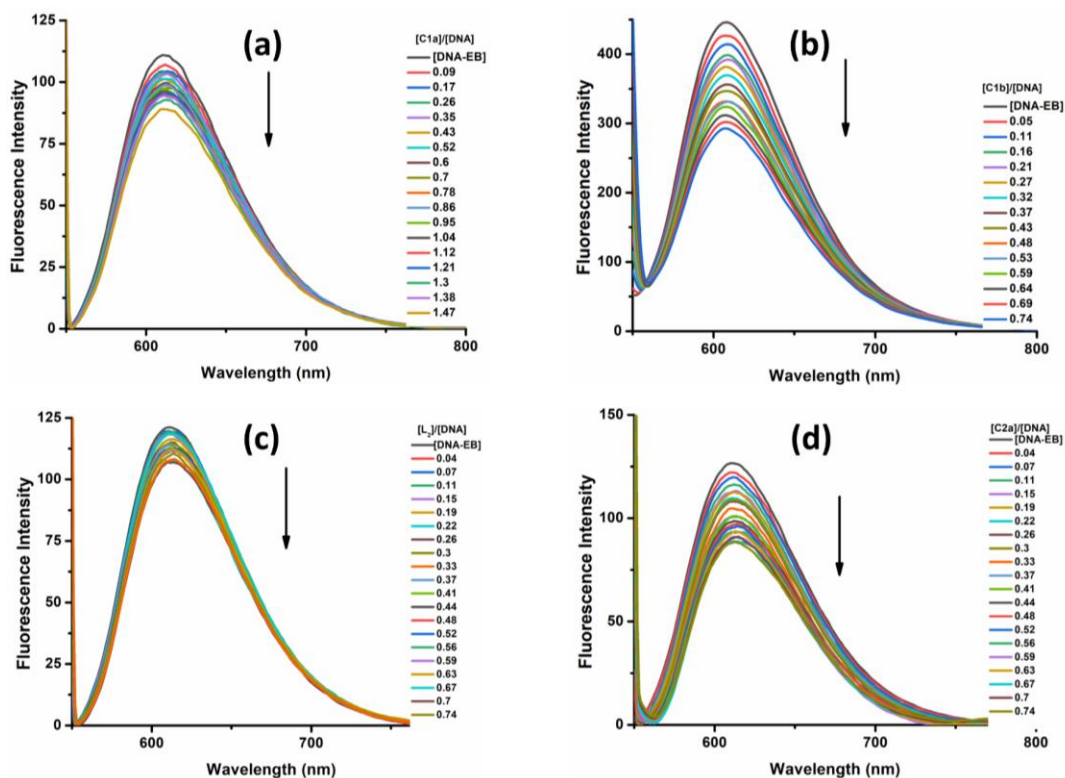


**Figure 6.2.4.3A** Fluorescence emission spectra of DNA-EB complex with increasing concentrations of (a)  $C1a$  (b)  $C1b$  (c)  $L^2$  (d)  $C2a$ . The arrow shows decrease in intensity (quenching of DNA-EB fluorescence) upon increasing concentration of the complex

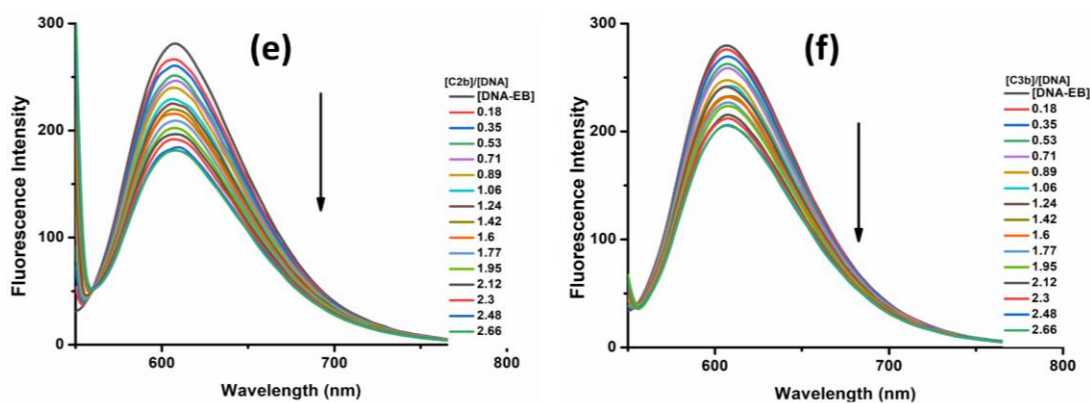


**Figure 6.2.4.3A (Contd...)** Fluorescence emission spectra of DNA-EB complex with increasing concentrations of (e)  $C2b$  (f)  $C3a$ . The arrow shows decrease in intensity (quenching of DNA-EB fluorescence) upon increasing concentration of the complex

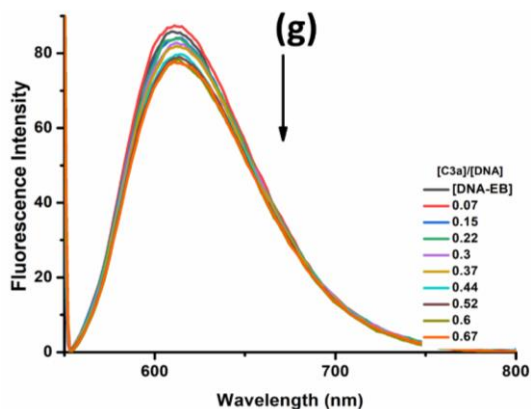


**Figure 6.2.4.3A (Contd...)** (g) Fluorescence emission spectra of DNA-EB complex with increasing concentrations of **C3b**. The arrow shows decrease in intensity (quenching of DNA-EB fluorescence) upon increasing concentration of the complex

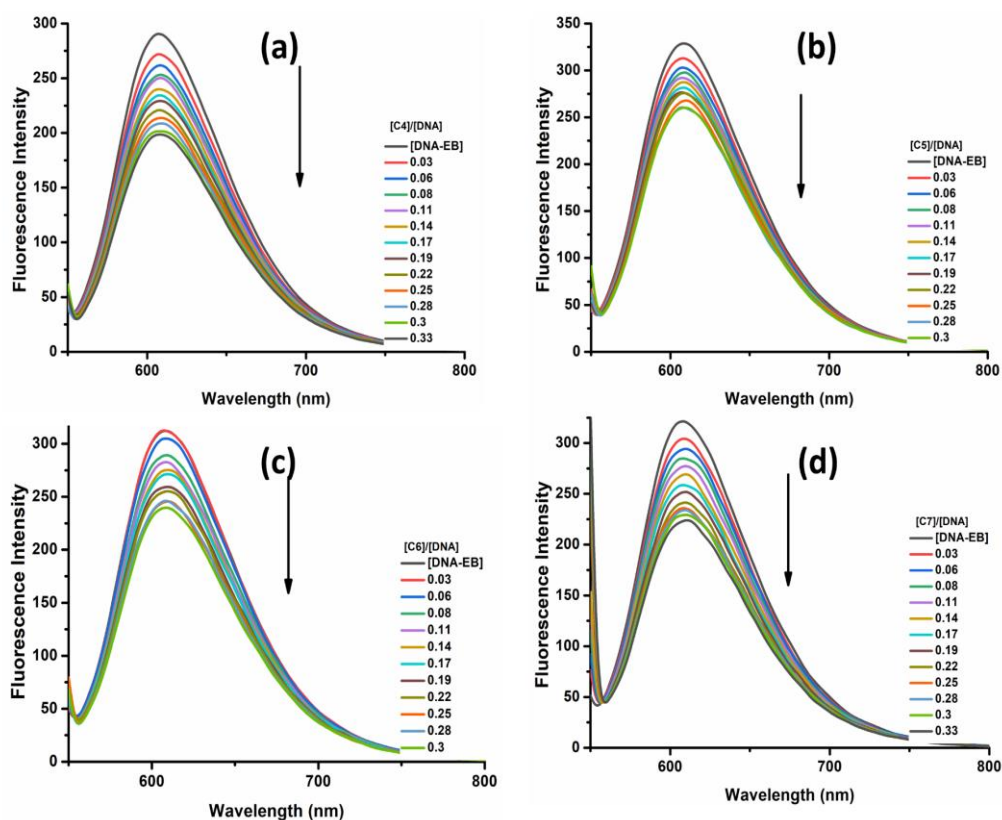


**Figure 6.2.4.3B** Fluorescence emission spectra of DNA-EB complex with increasing concentrations of (a) **C4** (b) **C5** (c) **C6** (d) **C7**. The arrow shows decrease in intensity (quenching of DNA-EB fluorescence) upon increasing concentration of the complex

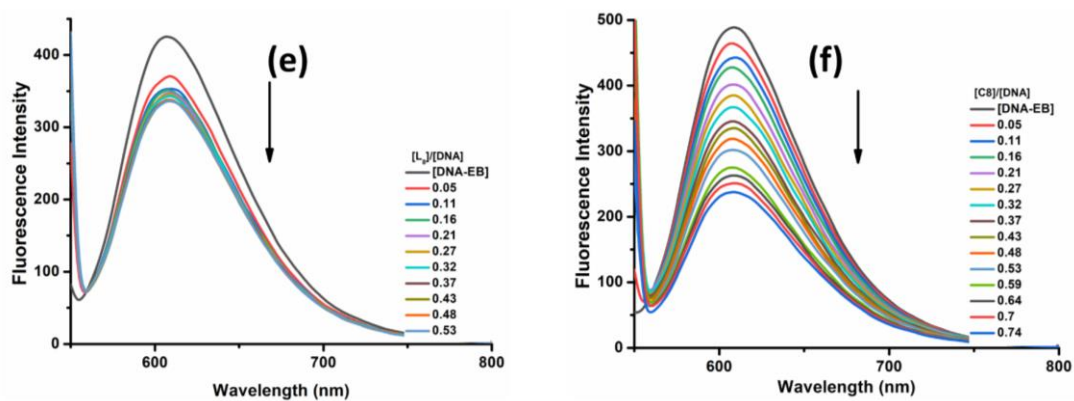


**Figure 6.2.4.3B (Contd..)** Fluorescence emission spectra of DNA-EB complex with increasing concentrations of (e)  $L^8$  and (f)  $C8$ . The arrow shows decrease in intensity (quenching of DNA-EB fluorescence) upon increasing concentration of the complex

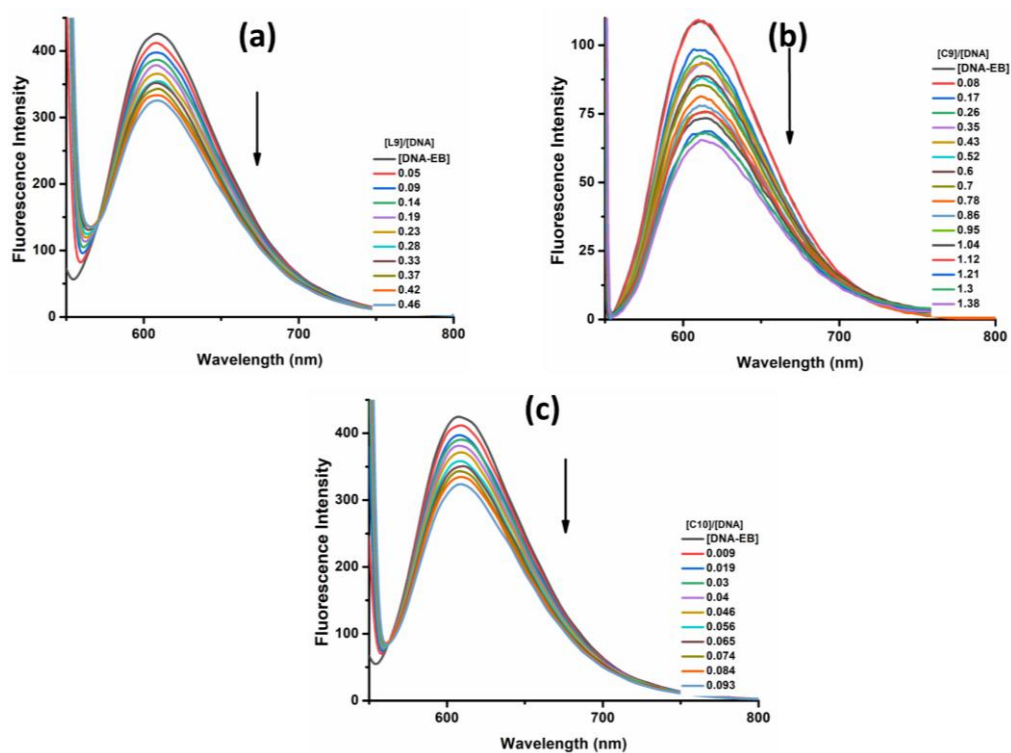


**Figure 6.2.4.3C** Fluorescence emission spectra of DNA-EB complex with increasing concentrations of (a)  $L^9$  (b)  $C9$  (c)  $C10$ . The arrow shows decrease in intensity (quenching of DNA-EB fluorescence) upon increasing concentration of the complex

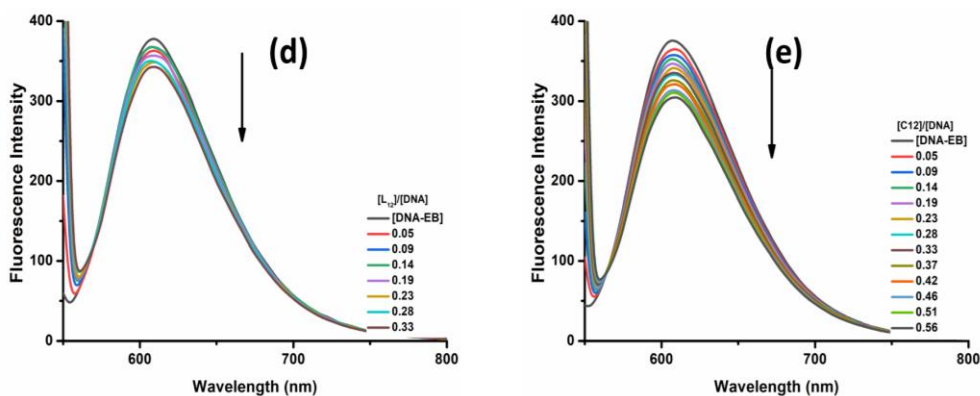


**Figure 6.2.4.3C (Contd.)** Fluorescence emission spectra of DNA-EB complex with increasing concentrations of (d)  $L^{12}$  and (e)  $C12$ . The arrow shows decrease in intensity (quenching of DNA-EB fluorescence) upon increasing concentration of the complex

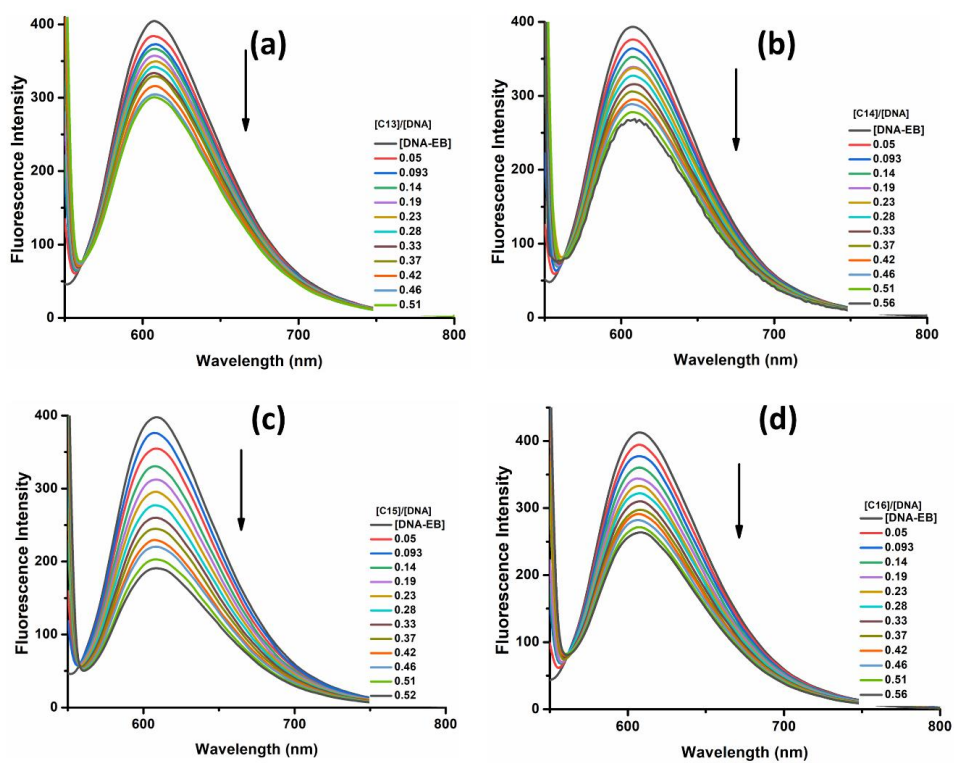


**Figure 6.2.4.3D** Fluorescence emission spectra of DNA-EB complex with increasing concentrations of (a)  $C13$  (b)  $C14$  (c)  $C15$  (d)  $L^{16}$  and (e)  $C16$ . The arrow shows decrease in intensity (quenching of DNA-EB fluorescence) upon increasing concentration of the complex

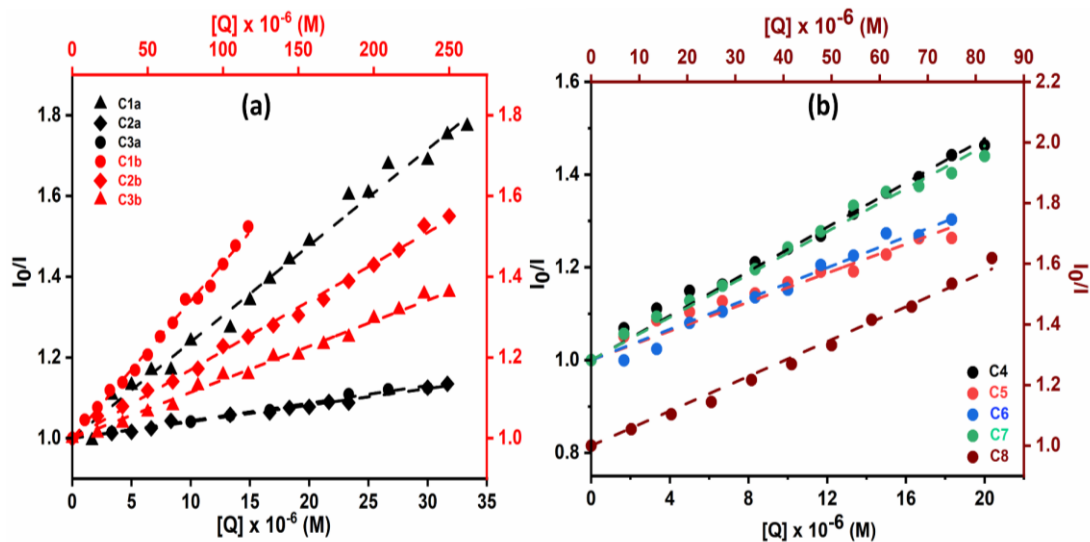


Figure 6.2.4.4A Stern-Volmer quenching plot,  $I_0/I$  versus  $[Q]$  of DNA-EB for complexes (a) C1a-C3a and C1b-C3b (b) C4-C8

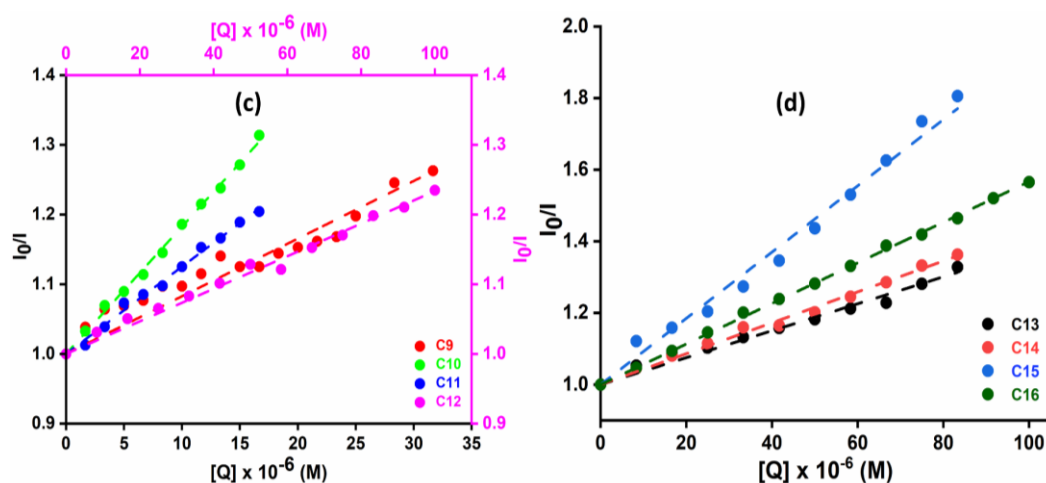


Figure 6.2.4.4B Stern-Volmer quenching plot,  $I_0/I$  versus  $[Q]$  of DNA-EB for complexes (c) C9, C10 and C12 (b) C13-C16

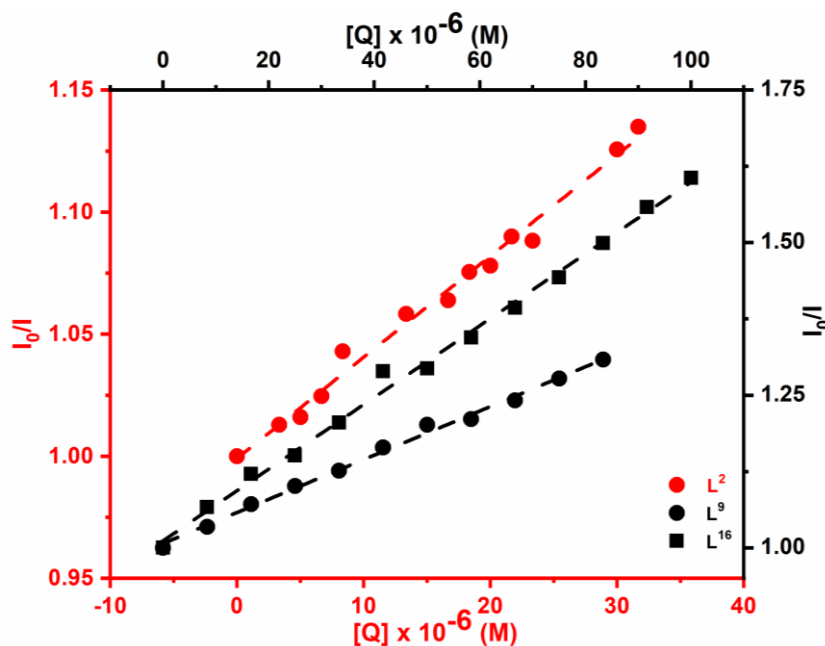


Figure 6.2.4.4C Stern-Volmer quenching plot,  $I_0/I$  versus  $[Q]$  of DNA-EB for ligands

#### 6.2.4 Results and Discussion

The  $K_b$  (intrinsic binding constant) values (Table 6.2.4.1) obtained from the plot of  $[DNA]/(\epsilon_A - \epsilon_F)$  versus  $[DNA]$  (Figure 6.2.4.2) using equation (6.1) are in the range of  $7.77 \times 10^3 - 1.646 \times 10^6$  M for complexes suggesting moderate binding of the complexes to ct-DNA. An observed hypochromism along with a bathochromic shift is indicative of intercalative mode of binding to the DNA. Out of all copper(II) complexes, complex **C10** and **C12** have the highest  $K_b$  values.

An overall comparison of values shows that the complexes have relatively stronger binding than the corresponding ligands with DNA. In the series of compounds derived from **dfc**, homonuclear dicopper(II) complexes have stronger binding with DNA as compared to the heteronuclear copper(II)-zinc(II) complexes. In the series of compounds derived from **dac**, complex **C7** has stronger binding with DNA as compared to the other dicopper(II) complexes of this series. In the compounds derived from **dap**, complex **C10** and **C12** have better DNA binding efficiencies. Among the dicopper(II) complexes derived from **bamnp**, the complexes **C14** and **C15** have stronger binding with DNA.

Competitive EB binding studies show quenching of DNA-EB fluorescence on titration with ligands and complexes suggesting that the compounds displace EB from DNA-EB complex and interact with DNA via intercalative mode. The Stern-

Volmer quenching plots of DNA-EB (**Figure 6.2.4.4A**) illustrate that the quenching of EB bound to DNA by the compounds is in good agreement ( $R^2 = 0.98-0.99$ ) with the linear Stern-Volmer equation (**6.2**). The  $K_{SV}$  values of the compounds given in **Table 6.2.4.1** show that they have good affinity for DNA with values in the range of  $0.14 - 2.41 \times 10^4$  M for all ligands and complexes.

It can be well noted that the homonuclear dicopper(II) complexes shows 10 fold better efficacies for displacement of EB from DNA-EB complexes than heteronuclear copper(II)zinc(II) complexes of ligands derived from **dfc**. This observation is in agreement with the  $K_b$  values obtained from UV absorption studies. This shows that along with planarity of aromatic rings of ligands, the metal ions also play a key role in binding with the DNA. In the complexes of ligands derived from **dac**, the complexes having more nitrogen rich ligands shows better efficacies for displacement of EB from DNA-EB complexes as compared to the other dicopper(II) complexes in the series. Thus, complex **C4** and **C7** shows better efficacies for displacement of EB. In the series of complexes derived from **dap**-based ligands, complex **C9** shows better efficiency for displacing EB from DNA-EB complex due to the aromatic naphthyl ring which has appropriate orientation bind with DNA via intercalation mode than other complexes of this series. Among the series of complexes derived from **bamnp**, complex **C15** has better efficiency for displacing EB from DNA-EB complex than other complexes of this series. This can be ascribed to the more planar aromatic rings in the complex.

**Table 6.2.4.1** DNA binding constants of ligands ( $L^2-L^3$ ,  $L^8$ ,  $L^9$  and  $L^{12}$ ) and complexes (**C1a-3a**, **C1b-3b**, **C4-C8**, **C9**, **C10**, **C12**, **C13-C16**)

Compound	DNA binding constants	
	$K_b$ M <sup>-1</sup>	$K_{SV}$ M <sup>-1</sup>
<b>DFC series</b>		
<b>L<sup>2</sup></b>	$2.465 \times 10^4$	$4 \times 10^3$
<b>L<sup>3</sup></b>	No binding	
<b>C1a</b>	$7.77 \times 10^3$	$4.3 \times 10^4$
<b>C1b</b>	$3.7056 \times 10^4$	$4.3 \times 10^3$
<b>C2a</b>	$5.5834 \times 10^4$	$1.4 \times 10^4$
<b>C2b</b>	$3.343 \times 10^4$	$2.1 \times 10^3$
<b>C3a</b>	$6.733 \times 10^4$	$4.8 \times 10^3$
<b>C3b</b>	$6.667 \times 10^4$	$1.4 \times 10^3$
<b>DAC series</b>		
<b>C4</b>	$2.455 \times 10^4$	$2.41 \times 10^4$
<b>C5</b>	$1.365 \times 10^4$	$1.61 \times 10^4$
<b>C6</b>	$2 \times 10^4$	$1.66 \times 10^4$

<b>C7</b>	$8.755 \times 10^4$	$2.39 \times 10^4$
<b>L<sup>8</sup></b>	$5.925 \times 10^3$	No binding
<b>C8</b>	$1.09 \times 10^4$	$7 \times 10^3$
<b>DAP series</b>		
<b>L<sup>9</sup></b>	$5.271 \times 10^4$	$3.7 \times 10^3$
<b>C9</b>	$1.00 \times 10^4$	$2 \times 10^4$
<b>L<sup>10</sup></b>	No binding	
<b>C10</b>	$1.646 \times 10^6$	$1.82 \times 10^4$
<b>L<sup>12</sup></b>	$3.973 \times 10^5$	No binding
<b>C12</b>	$1.509 \times 10^6$	$2.3 \times 10^3$
<b>BAMNP series</b>		
<b>C13</b>	$2.22 \times 10^4$	$3.8 \times 10^3$
<b>C14</b>	$3.002 \times 10^4$	$4.3 \times 10^3$
<b>C15</b>	$2.779 \times 10^4$	$9 \times 10^3$
<b>L<sup>16</sup></b>	No binding	
<b>C16</b>	$2.291 \times 10^4$	$5.7 \times 10^3$

### 6.3 Interaction with proteins - BSA binding studies

#### 6.3.1 Serum Albumin: an important biomolecule

Albumin is the most important and abundant protein in the blood plasma of all vertebrates with the concentration in human serum being 35-50mg/ml and a molecular weight of 66.5kDa. It is stable in the pH range of 4-9, soluble in 40% ethanol, and can be heated at 60°C for up to 10 hours without deleterious effects. Serum albumin becomes an ideal candidate for drug delivery<sup>34</sup> due to these properties, as well as preferential uptake in tumor and inflamed tissue, ready availability, biodegradability, and lack of toxicity and immunogenicity.

Human Serum Albumin (HSA) is composed of three homologous domains, numbered I, II and III.<sup>35</sup> Each domain is grouped into subdomains A and B that possess common structural motifs.

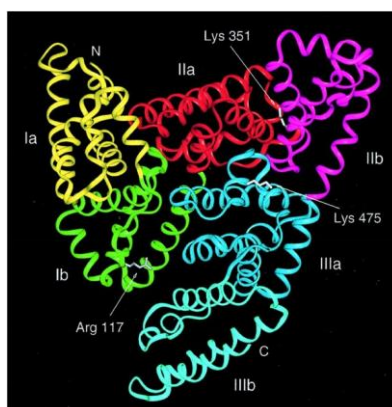


**Figure 6.3.1.1** Structure of human serum albumin consisting of three domains, each grouped into subdomains A and B

The two principal regions responsible for the ligand-binding to HSA have been known as Sudlow's Site I and II, located in subdomain IIA and IIIA (**Figure 6.3.1.1**), respectively.<sup>36,37</sup>

Albumin can bind various endogenous molecules, including long-chain fatty acids, steroids, L-tryptophan, etc. Moreover, albumin is also involved in transporting ions in the circulation, including copper, zinc, calcium, etc. Additionally, this vital protein can bind exogenous compounds and drugs, such as warfarin, ibuprofen, chlorpromazine and naproxen, with the affinity of their binding significantly affecting their activity and half-life.<sup>37-39</sup> Albumin is present in extravascular space (~ 242g) predominantly rather than the intravascular space (~118g). The extracellular locations where these proteins are present include skin, gut, muscle, other fluids and secretions along with low concentrations in intracellular locations. The proteins return to circulation from extracellular spaces *via* lymphatic system, approx. 28 trips in and out during its lifetime.<sup>38,39</sup>

It is a versatile and captivating protein. It is considered as biocompatible and biodegradable carrier of drugs due to demonstration of its recent applications in biomedical sciences.<sup>40-42</sup> The search and characterization of albumin-binding drugs, particularly in cancer cells, is of considerable interest in light of the development of albumin as an effective drug carrier to target tumors. Albumin-binding may provide an advantage when generating tumor targeting agents and this requires further intense investigation. Hence is the present effort to evaluate the complex-BSA interaction.

### **6.3.2 Materials and instrumentation**

The BSA (Bovine Serum Albumin) binding studies were solely carried out in tris buffer tris(hydroxymethyl)-aminomethane-HCl (15 mM)/NaCl (150 mM) buffer (pH adjusted to 7.5 with conc. HCl prepared in double distilled water). BSA stock solution was prepared in double distilled water with a concentration of  $28.35 \times 10^{-6}$  M. The stock solutions of all the compounds under study were prepared in neat DMSO with a stock concentration of  $10^{-3}$  M. BSA was purchased from Hi-media, Mumbai, India.

Fluorescence spectra were recorded in tris buffer solution at concentrations of  $10^{-6}$  M on JASCO FP-6300 fluorescence spectrophotometer.

The data generated from the titration experiments were analyzed and plotted with the help of the software Origin2019b.

### **6.3.3 Experimental section**

Bovine serum albumin (BSA) is extensively studied, due to its structural homology with human serum albumin (HSA). HSA contains 585 amino acid residues with only one tryptophan located at position 214, while BSA has two tryptophans at positions 134 and 212 along the chain (**Figure 6.3.3.1**). BSA solutions exhibit a strong fluorescence emission with a peak at 343 nm, due to the tryptophan residues, when excited at 296 nm. The interaction of compounds with BSA has been studied from tryptophan emission-quenching experiments. The changes in the emission spectra of tryptophan in BSA are primarily due to changes in protein conformation, subunit association, substrate binding or denaturation [67,68]. Addition of a compound to a solution of BSA results in a decrease of the fluorescence intensity because of their binding to BSA which may change the protein secondary structure leading to changes in the tryptophan environment of BSA. The protein-binding study for the dicopper(II) complexes was performed by tryptophan fluorescence quenching experiments using bovine serum albumin (BSA) in buffer. The quenching of emission intensity of the tryptophan residues of BSA at 343 nm was monitored in the presence of increasing concentrations of complexes as quenchers. Fluorescence spectra were recorded from 300 to 500 nm at an excitation wavelength of 296 nm. The titration curve so generated has been representatively shown in **Figure 6.3.4.1**. But the addition of compound to a solution of BSA results in an increase of the fluorescence intensity because of their binding of BSA which changes the protein secondary structure leading to change in tryptophan residues. The enhanced emission intensity of the tryptophan residues of BSA at 343nm was monitored in presence of increasing concentrations of complexes as fluorophore. The titration curve so generated has been representatively shown in **Figure 6.3.4.1A(d)** and **Figure 6.3.4.1B(e,f)**.

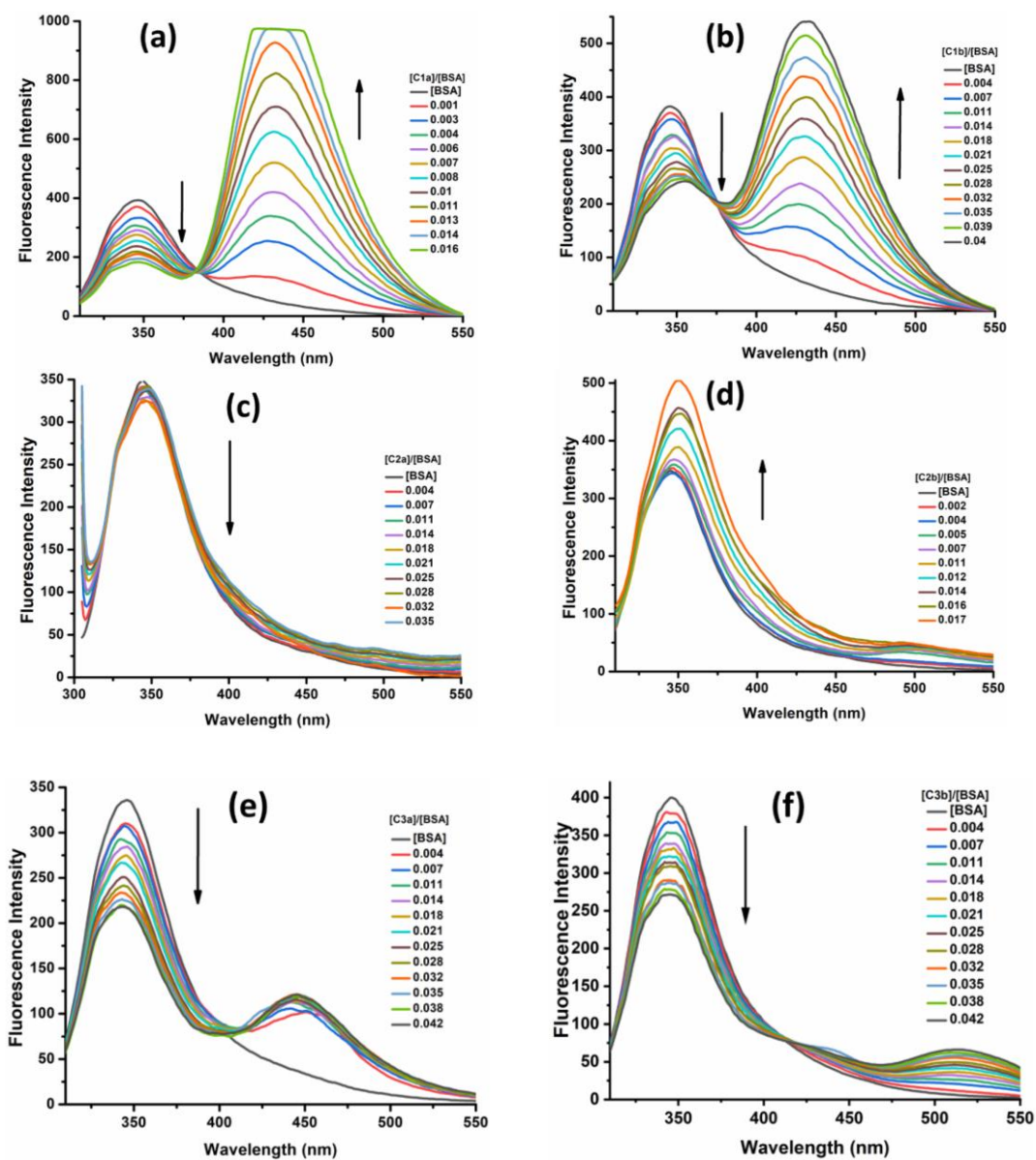


**Figure 6.3.4.1A** Fluorescence emission spectra of BSA with increasing concentrations of (a) C1a (b) C1b (c) C2a (d) C2b (e) C3a and (f) C3b. The arrow shows decrease in intensity (quenching of BSA fluorescence) upon increasing concentration of the complex except complex C2b

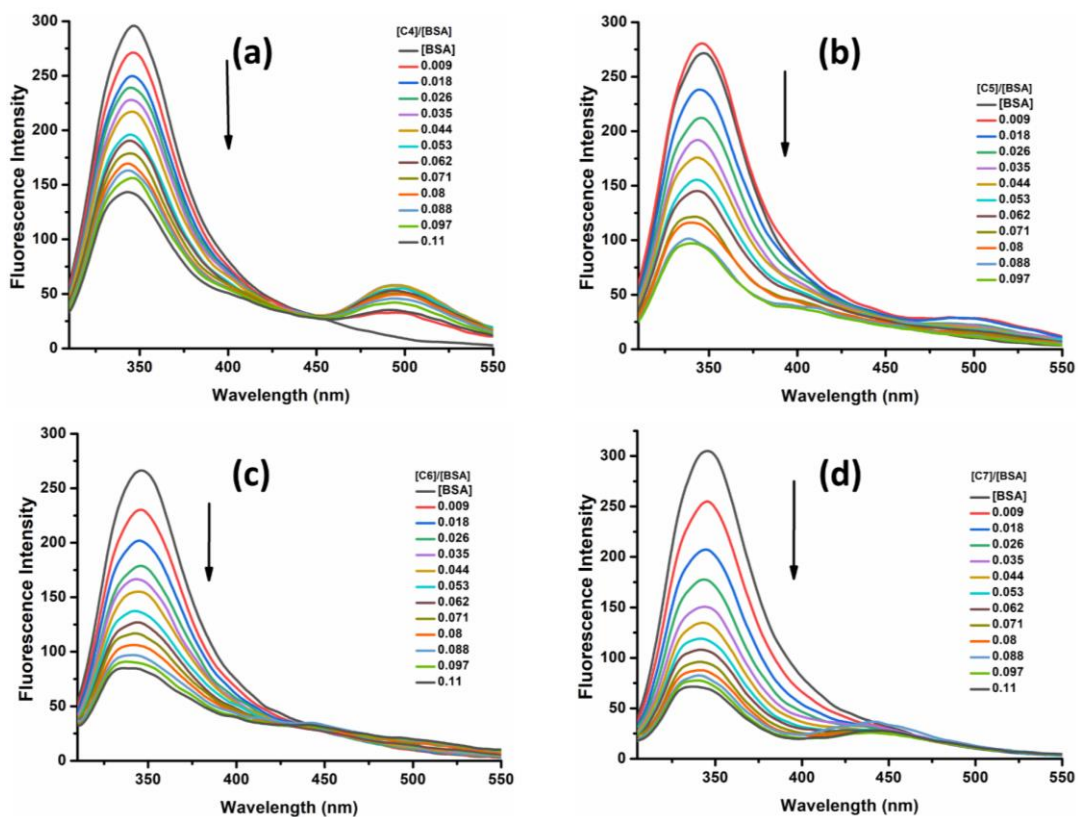


**Figure 6.3.4.1B** Fluorescence emission spectra of BSA at increasing concentrations of (a) C4 (b) C5 (c) C6 and (d) C7, the arrow shows decrease in intensity (quenching of BSA fluorescence) upon increasing concentration of the complex

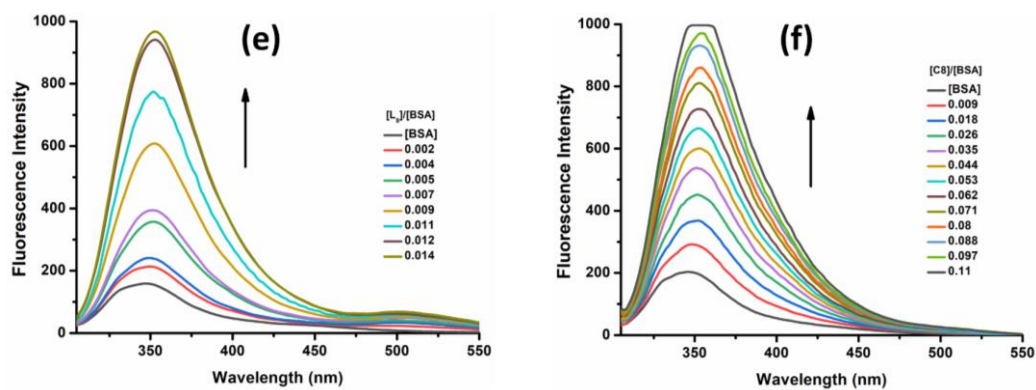


**Figure 6.3.4.1B** (Contd....) Fluorescence emission spectra of BSA at increasing concentrations of (e) L<sub>8</sub> and (f) C<sub>8</sub>, the arrow shows increase in intensity (enhancing of BSA fluorescence) upon increasing concentration of the complex

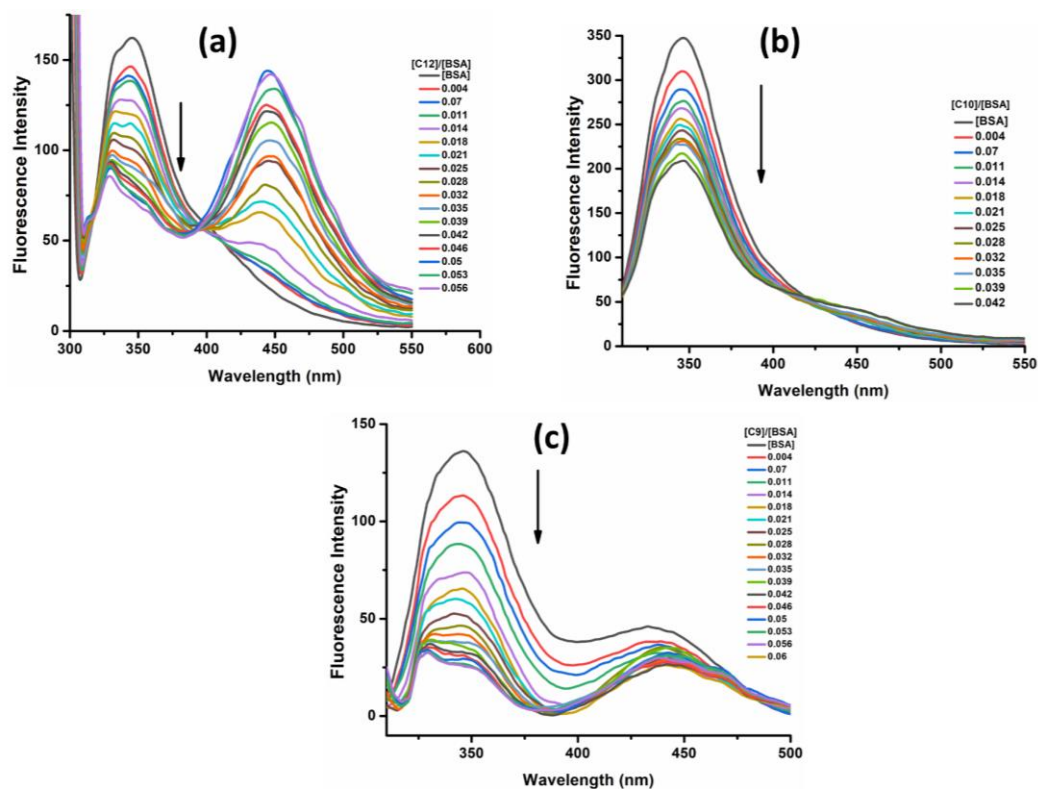


**Figure 6.3.4.1C** Fluorescence emission spectra of BSA at increasing concentrations of (a) C9 (b) C10 and (c) C12, the arrow shows decrease in intensity (quenching of BSA fluorescence) upon increasing concentration of the complex

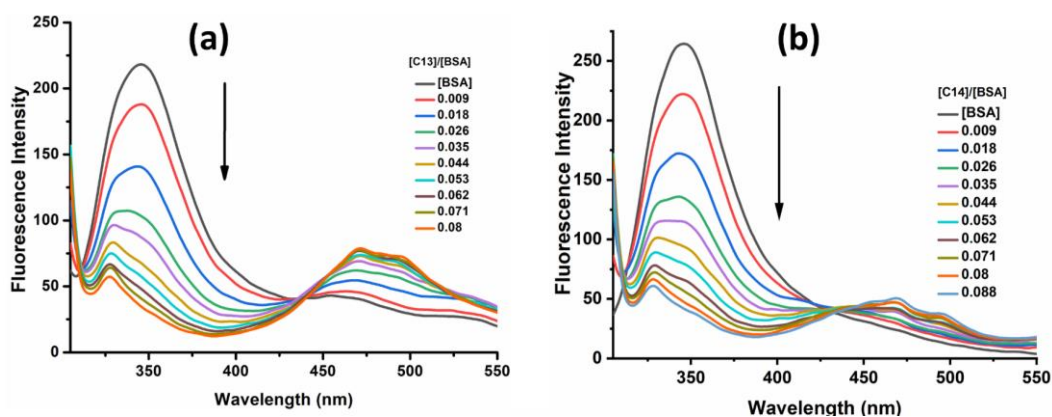


**Figure 6.3.4.1D** Fluorescence emission spectra of BSA at increasing concentrations of (a) C13 (b) C14, the arrow shows decrease in intensity (quenching of BSA fluorescence) upon increasing concentration of the complex

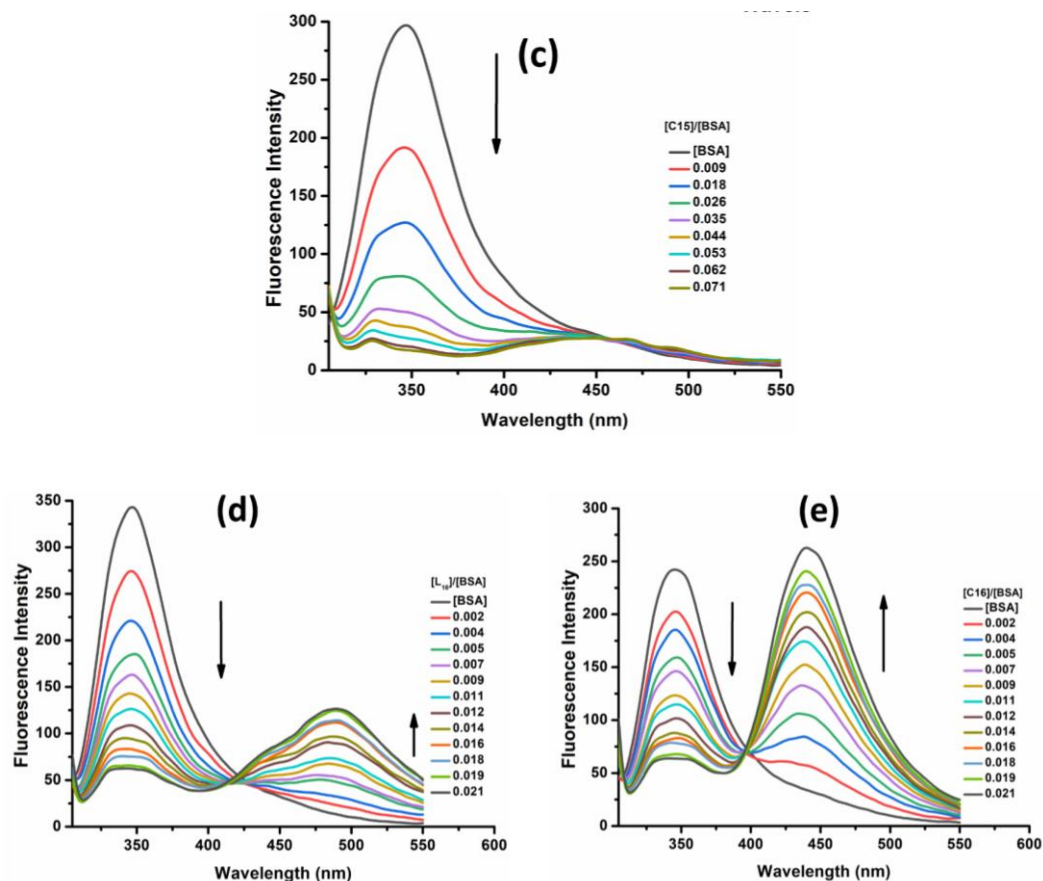


**Figure 6.3.4.1D (Contd.)** Fluorescence emission spectra of BSA at increasing concentrations of (c) C15 (d) L<sup>16</sup> and (e) C16, the arrow shows decrease in intensity (quenching of BSA fluorescence) upon increasing concentration of the complex

The Stern–Volmer equation (6.2) may be used in order to study the interaction of a quencher with serum albumins.

$$I_0/I = 1 + K_{SV}[Q] \quad (6.2)$$

where  $I_0$  is the initial tryptophan fluorescence intensity of BSA,  $I$  is the tryptophan fluorescence intensity of BSA after the addition of the quencher and  $K_{SV}$  the dynamic quenching constant. The dynamic quenching constant ( $K_{SV} \text{ M}^{-1}$ ) can be obtained from the slope of the plot  $I_0/I$  versus  $[Q]$ . The  $K_{SV}$  plots for all the synthesized ligands (except ligand L<sub>16</sub> in Figure 6.3.4.3C) and their corresponding copper(II) complexes have been shown in Figure 6.3.4.2. The  $K_{SV}$  values obtained from these plots have been tabulated and discussed in section 6.3.4.

The following equation was used to determine the bimolecular quenching rate constant  $K_q$ :

$$K_q = K_{SV}/\tau_0 \quad (6.3)$$

where  $K_{SV}$  is the Stern-Volmer constant and  $\tau_0$  is the average lifetime of the fluorophore in the absence of the quencher ( $\tau_0 = 10$  ns for BSA).

The equation (6.4) may be used in order to study the interaction of a compound with serum albumins.

$$I/I_0 = 1 + K_a[Q] \quad (6.4)$$

where  $I_0$  is the initial tryptophan fluorescence intensity of BSA,  $I$  is the tryptophan fluorescence intensity of BSA after the addition of the complex and  $K_a$  = the binding constant. The binding constant ( $K_a \text{ M}^{-1}$ ) can be obtained from the slope of the plot  $I/I_0$  versus  $[Q]$ . The  $K_a$  plots for synthesized ligand **L8** and copper(II) complexes (**C2b** and **C8**) have been shown in **Figure 6.3.4.2**. The  $K_{SV}$  values obtained from these plots have been tabulated and discussed in **section 6.3.4**.

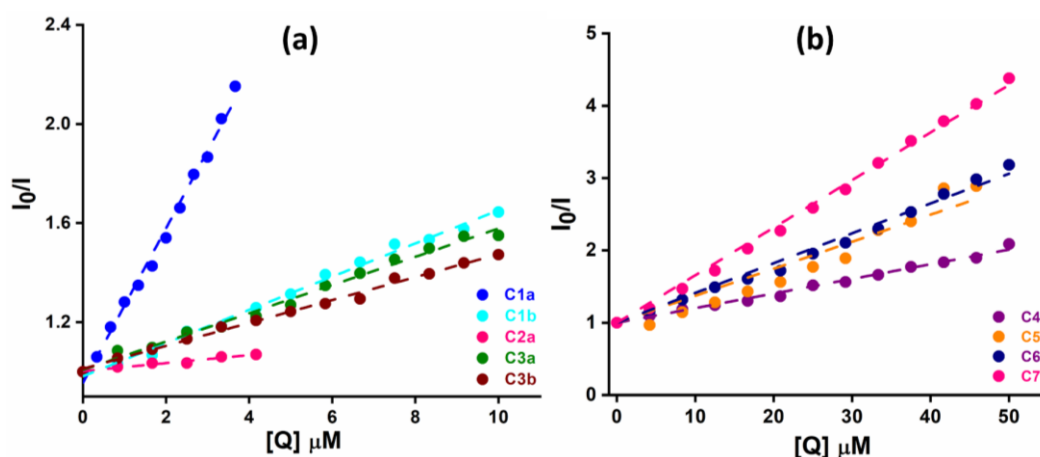


**Figure 6.3.4.2A** Stern-Volmer quenching plot  $I_0/I$  versus  $[Q]$  of BSA for (a) **C1a-C3a** and **C1b-C3b** (**C2a**-no binding and **C2b**- enhancement in fluorescence) and (b) **C4-C7**

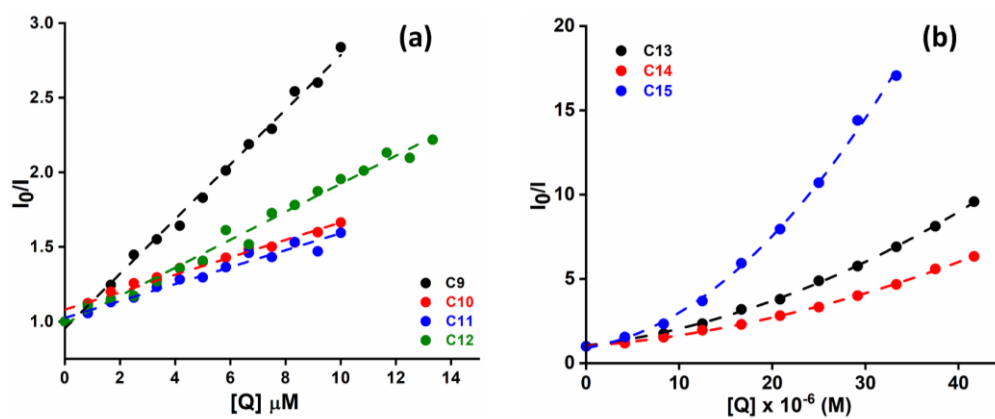


Figure 6.3.4.2B Stern-Volmer quenching plot  $I_0/I$  versus  $[Q]$  of BSA for (a) C9, C10 and C12 and (b) C13-C15

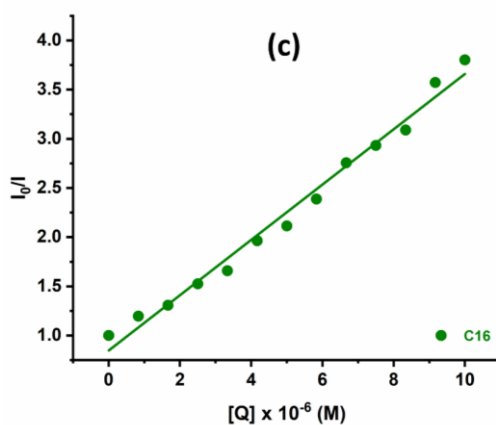


Figure 6.3.4.2B (Contd..) Stern-Volmer quenching plot  $I_0/I$  versus  $[Q]$  of BSA for (c) C16

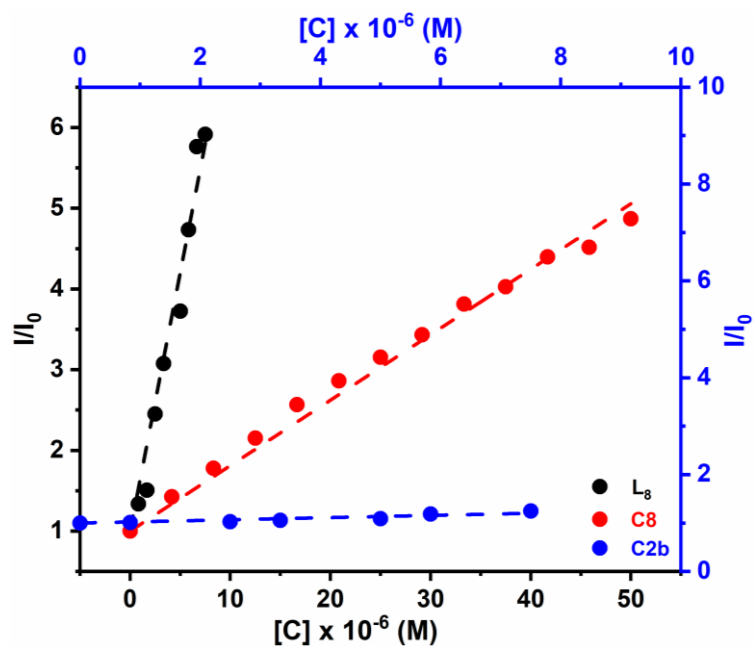


Figure 6.3.4.2C Plot of  $I/I_0$  versus  $[C]$  of BSA for ligand  $L^8$  and Complexes (C2b and C8)

Quenching of emission in the fluorescence spectra may be owing to a variety of molecular interactions including excited-state reactions through collisional quenching, energy transfer, ground state complex formation and molecular rearrangements. The different mechanisms of quenching are usually classified as:

- Static quenching (the formation of a complex between quencher and fluorophore)
- Dynamic quenching (a collisional process).

The type of quenching mainly operating in the systems can be speculated from the nature of the Stern–Volmer plots. Linear Stern–Volmer plots (**Figure 6.3.4.2**) represent a single quenching mechanism, either static or dynamic although which mechanism is operative cannot be speculated. Sometimes a nonlinear Stern–Volmer plot with an upward, concave curvature towards the y-axis at high [Q] may result, if both static and dynamic quenching processes are operating simultaneously in an interacting system.

When small molecules are bound independently to a set of equivalent sites on a macromolecule, the equilibrium between free and bound molecules is given by double-logarithm equation (6.4) [69]. This equation has been employed to determine the binding constant ( $K_a$ ) and the number of binding sites ( $n$ ) for complex–BSA interaction.

$$\log ((I_0 - I)/I) = \log K_a + n \log [Q] \quad (6.4)$$

where  $I_0$  and  $I$  are the fluorescence intensities in the absence and the presence of quencher, and [Q] is the concentration of quencher (copper(II) complexes). The plot of  $\log [(I_0 - I)/I]$  versus  $\log [Q]$  for all the systems is linear (**Figure 6.3.4.3**) indicating the operation of a single quenching mechanism. The values of  $K_a$  and  $n$  have been obtained from the intercept and slope, respectively, which have been tabulated and discussed in **section 6.3.4**.

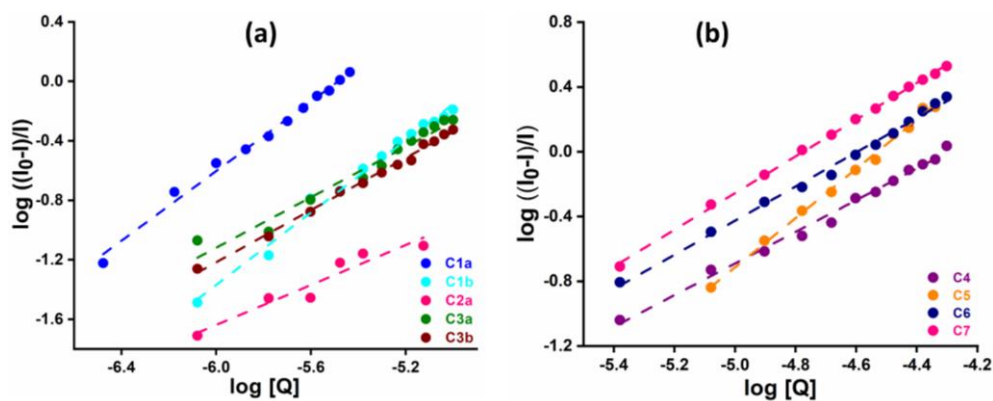


**Figure 6.3.4.3A** Double logarithmic plot for the quenching of BSA fluorescence by (a) C1a-C3a and C1b-C3b (C2a-no binding and C2b- enhancement in fluorescence) and (b) C4-C7

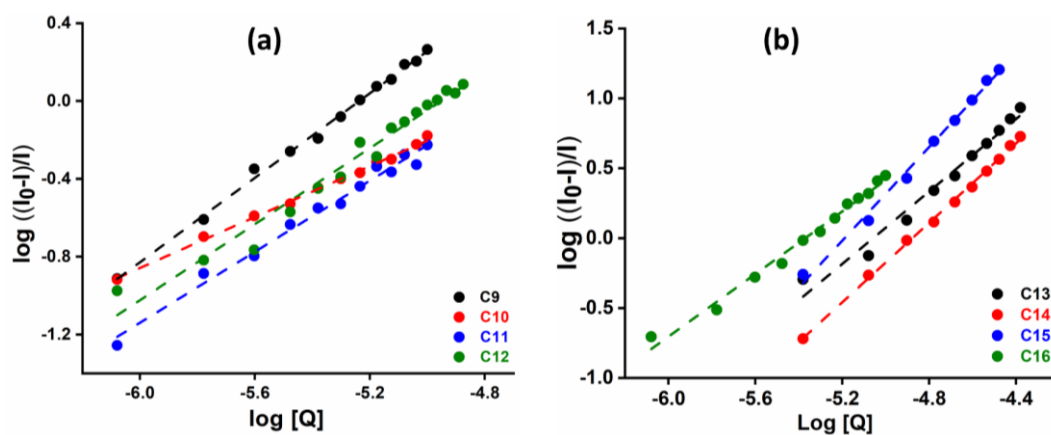


**Figure 6.3.4.3B** Double logarithmic plot for the quenching of BSA fluorescence by (a) C9, C10 and C12 and (b) C13-C16

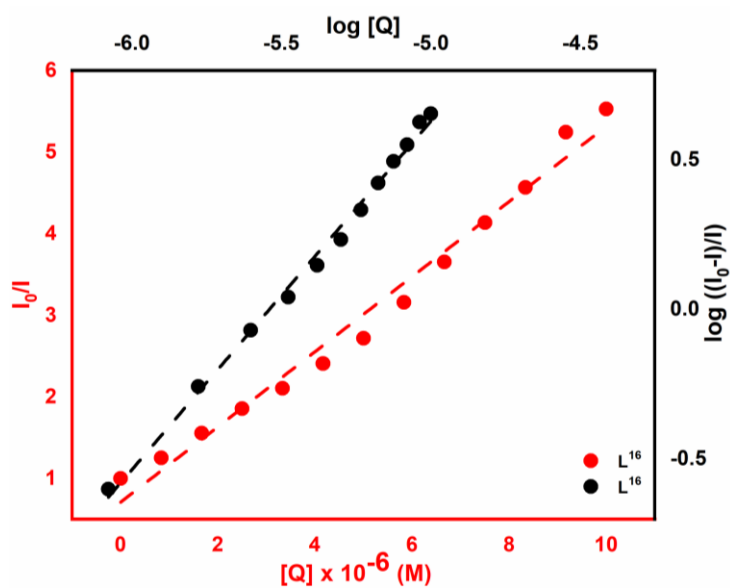


**Figure 6.3.4.3C** Stern-Volmer plot and Double logarithmic plot for the quenching of BSA fluorescence of ligand  $L^{16}$

## BSA Conformational analysis

Synchronous fluorescence spectra of BSA in presence of copper(II) complexes was also recorded using the same concentrations at two different  $\Delta\lambda$  values (difference between excitation and emission wavelengths of BSA) of 15 and 60 nm.

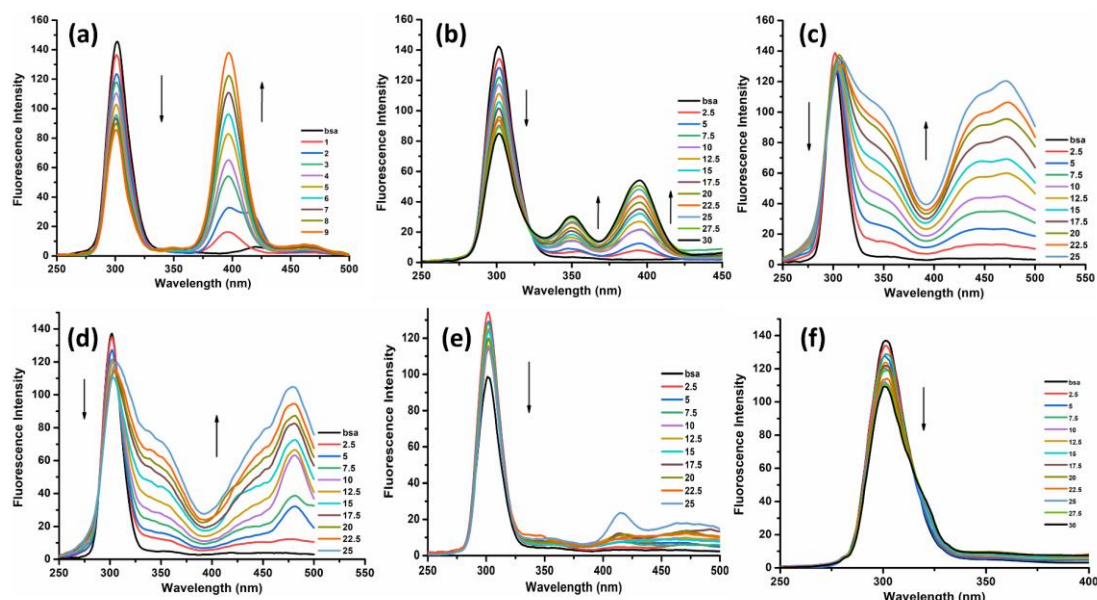


**Figure 6.3.4A** Synchronous BSA spectra in tris-HCl/NaCl buffer (pH=7.5) in presence of increasing concentrations of (a) C1a, (b) C1b, (c) C2a, (d) C2b, (e) C3a, and (f) C3b, at  $\Delta\lambda = 15$  nm (the downward arrow signifies a decrease in fluorescence intensity with increasing concentration of quencher)

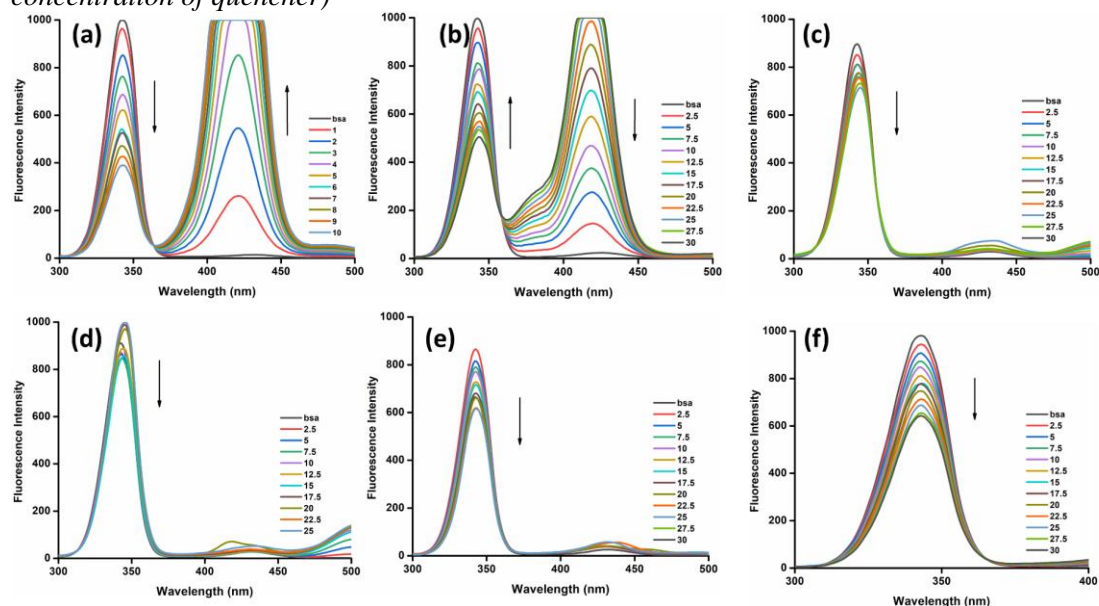


**Figure 6.3.4B** Synchronous BSA spectra in tris-HCl/NaCl buffer (pH=7.5) in presence of increasing concentrations of (a) C1a, (b) C1b, (c) C2a, (d) C2b, (e) C3a, and (f) C3b, at  $\Delta\lambda = 60$  nm (the downward arrow signifies a decrease in fluorescence intensity with increasing concentration of quencher)

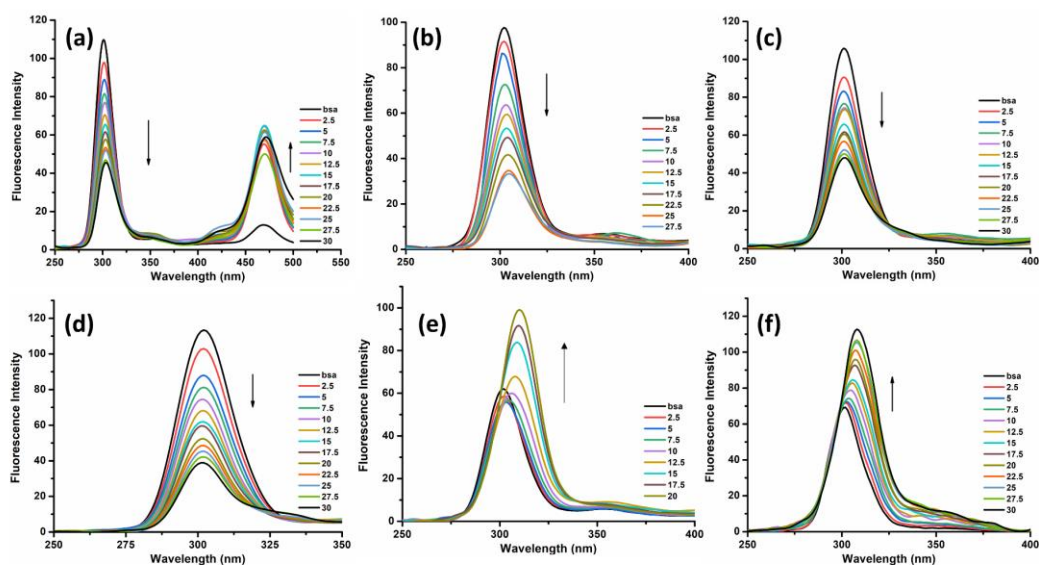


**Figure 6.3.4.4C** Synchronous BSA spectra in tris-HCl/NaCl buffer (pH=7.5) in presence of increasing concentrations of (a) C4, (b) C5, (c) C6, (d) C7, (e) L<sup>8</sup>, and (f) C8, at  $\Delta\lambda = 15 \text{ nm}$  (the downward arrow signifies a decrease in fluorescence intensity with increasing concentration of quencher)

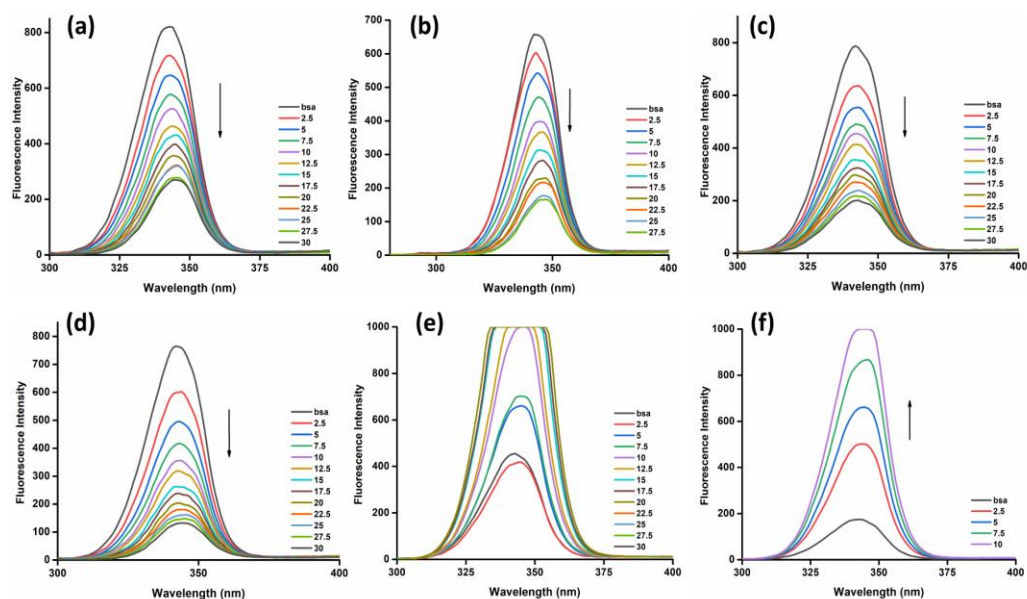


**Figure 6.3.4.4D** Synchronous BSA spectra in tris-HCl/NaCl buffer (pH=7.5) in presence of increasing concentrations of (a) C4, (b) C5, (c) C6, (d) C7, (e) L<sup>8</sup>, and (f) C8, at  $\Delta\lambda = 60 \text{ nm}$  (the downward arrow signifies a decrease in fluorescence intensity with increasing concentration of quencher)

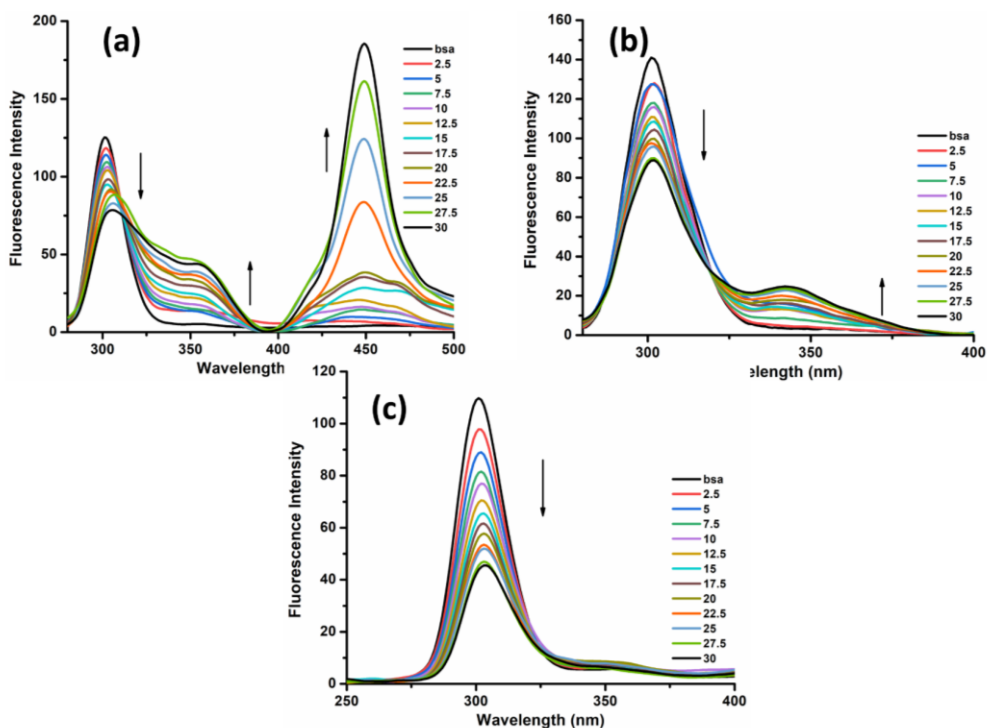


**Figure 6.3.4.4E** Synchronous BSA spectra in tris-HCl/NaCl buffer (pH=7.5) in presence of increasing concentrations of (a) C9, (b) C10, and (c) C12, at  $\Delta\lambda = 15 \text{ nm}$  (the downward arrow signifies a decrease in fluorescence intensity with increasing concentration of quencher)

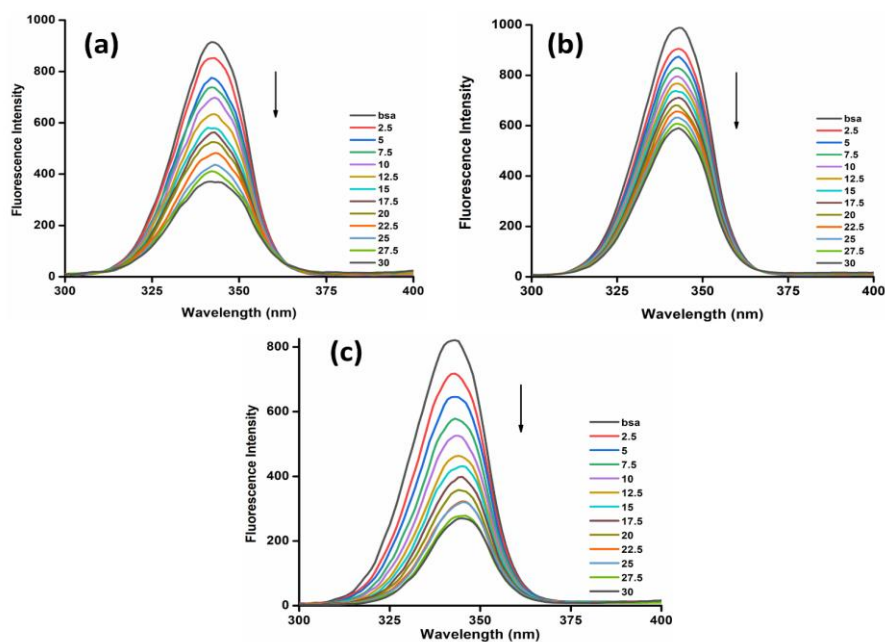


**Figure 6.3.4.4F** Synchronous BSA spectra in tris-HCl/NaCl buffer (pH=7.5) in presence of increasing concentrations of (a) C9, (b) C10, and (c) C12, at  $\Delta\lambda = 60 \text{ nm}$  (the downward arrow signifies a decrease in fluorescence intensity with increasing concentration of quencher)

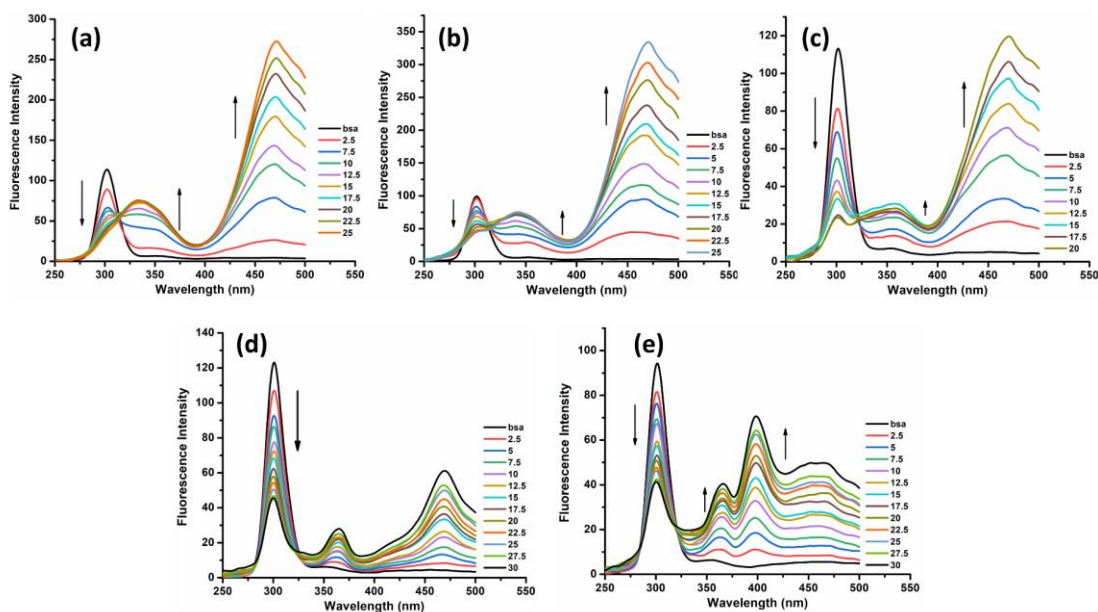


**Figure 6.3.4.4G** Synchronous BSA spectra in tris-HCl/NaCl buffer (pH=7.5) in presence of increasing concentrations of (a) C13, (b) C14, (c) C15, (d) L<sup>16</sup> and (e) C16, at  $\Delta\lambda = 15$  nm (the downward arrow signifies a decrease in fluorescence intensity with increasing concentration of quencher)

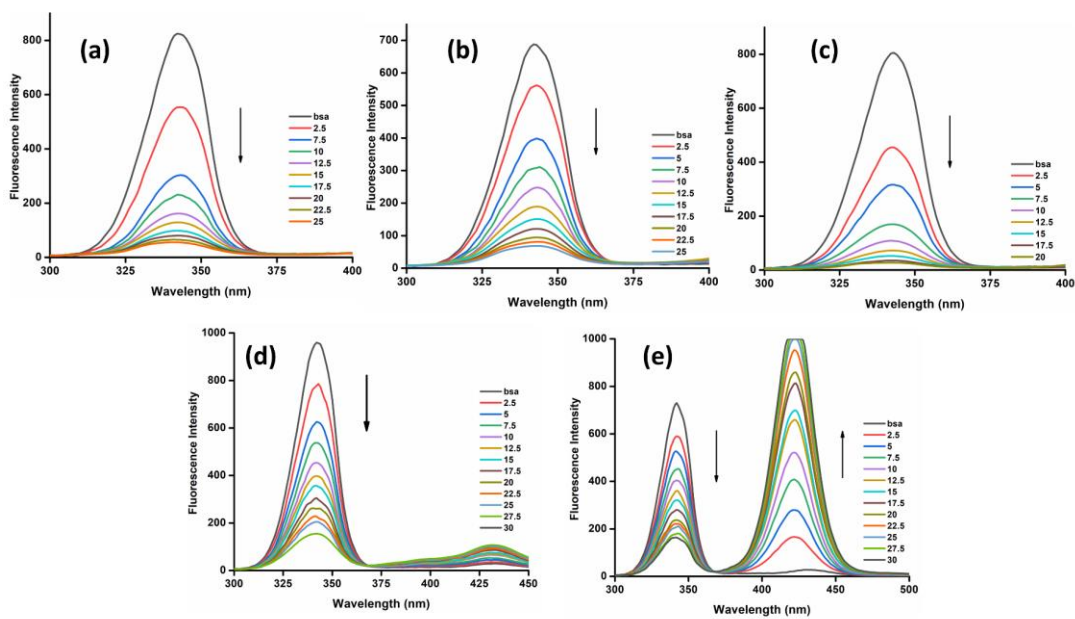


**Figure 6.3.4.4H** Synchronous BSA spectra in tris-HCl/NaCl buffer (pH=7.5) in presence of increasing concentrations of (a) C13, (b) C14, (c) C15, (d) L<sup>16</sup> and (e) C16, at  $\Delta\lambda = 60$  nm (the downward arrow signifies a decrease in fluorescence intensity with increasing concentration of quencher)

### 6.3.4 Result and Discussion

The binding interactions of the compounds under study with BSA led to quenching of its fluorescence. The Stern–Volmer plots (**Figure 6.3.4.2**) show that the curves have fine linear relationships ( $R^2 = 0.99$ ) according to the Stern–Volmer quenching equation (6.2) indicative of a single quenching process in the system but in complex **C13-C15**, the Stern-Volmer plots shows that an exceptional upward curve indicating the presence of dual quenching processes which is also evident from highest  $K_{SV}$  values among their respective series. The Stern-Volmer quenching constants  $K_{SV}$  (**Table 6.3.4.1**) calculated using equation (6.2) show that copper(II) complexes are having good binding propensity with BSA.

**Table 6.3.4.1** BSA binding constants of ligands ( $L^8$  and  $L^{16}$ ) and complexes (**C1a-3a**, **C1b-3b**, **C4-C8**, **C9**, **C10**, **C12**, **C13-C16**)

Compound	BSA binding constants			
	$K_{SV} (10^5 M^{-1})$	$K_q (10^{13} M^{-1} s^{-1})$	$K_a (10^5 M^{-1})$	n
<b>DFC series</b>				
<b>C1a</b>	2.947	2.947	26.466	1.171
<b>C1b</b>	0.644	0.644	8.45	1.216
<b>C2a</b>	No binding			
<b>C2b</b>	$K_a = 4.410 \times 10^4 (M^{-1})$			
<b>C3a</b>	0.582	0.582	0.0093	0.8484
<b>C3b</b>	0.48	0.48	0.1107	0.8768
<b>DAC series</b>				
<b>C4</b>	0.202	0.202	0.156	0.9768
<b>C5</b>	0.374	0.374	77.70	1.5201
<b>C6</b>	0.412	0.412	0.924	1.0807
<b>C7</b>	0.658	0.658	1.9231	1.1051
<b>L<sup>8</sup></b>	$K_a = 7.216 \times 10^5 (M^{-1})$			
<b>C8</b>	$K_a = 8.110 \times 10^4 (M^{-1})$			
<b>DAP series</b>				
<b>C9</b>	1.765	1.765	4.785	1.0847
<b>C10</b>	0.70	0.70	0.0117	0.6542
<b>C12</b>	0.922	0.922	0.6828	0.9763
<b>BAMNP series</b>				
<b>C13</b>	1.762	1.762	35.752	1.2957
<b>C14</b>	1.106	1.106	85.251	1.4211
<b>C15</b>	4.0720	4.0720	47918	1.6728
<b>L<sup>16</sup></b>	0.4189	0.4189	28.307	1.1643
<b>C16</b>	0.2593	0.2593	0.0117	0.6542

Quantitative binding to BSA was achieved using a double logarithmic plot. The plots of  $\log [(I_0-I)/I]$  versus  $\log [Q]$  for the present system are linear (**Figure 6.3.4.3**) and the values of  $K_a$  and  $n$  have been tabulated in **Table 6.3.4.1**. The  $K_a$  values confirm

---

that copper(II) complexes show much better binding efficacies after complexation with ligands.

The  $n$  values for all the complexes average out to be 1 which suggests that there is one binding site available on the protein.

### BSA conformational analysis

In order to get an information about the molecular microenvironment in the vicinity of the fluorophores, synchronous fluorescence spectra of BSA were recorded in presence of the synthesized copper(II) complexes. This study can indicate the possibility of binding with different amino acid residues in the proteins when the spectra are recorded at different  $\Delta\lambda$  values corresponding to different nature of chromophores; for a  $\Delta\lambda$  value of 15 nm, the fluorescence of BSA is characteristic of tyrosine residue, while a  $\Delta\lambda$  value of 60 nm, it corresponds to the tryptophan residue. The quenching of BSA fluorescence was monitored through a simultaneous scanning at wavelength difference of 15 nm and 60 nm. The synchronous BSA spectra for various concentrations of complexes at  $\Delta\lambda = 15\text{nm}$  (**Figure 6.3.4.4 A, C, E, G**) shows a decrease in the fluorescence intensity at 300 nm with a minor shift of 0-10 nm. The decrease in fluorescence intensity as compared to the initial values was observed to be ~ 20-45% for **C1-C3**, ~50-70% for **C4-C7**, ~35-60% for **C9, C10, C12**, and ~50-82% for **C13-C16** while the increase in fluorescence was observed for ligand **L<sub>8</sub>** and complex **C8** due to tryptamine part of ligand, which leads to enhancement of fluorescence in both.

The spectra at  $\Delta\lambda = 60\text{ nm}$  (**Figure 6.3.4.4 B, D, F, H**) for increasing concentrations of complexes also showed a regular and significant decrease in the intensity at 341 nm, upto ~ 29-60% for **C1-C3**, ~70-80% for **C4-C7**, ~40-70% for **C9, C10, C12**, and ~80-97% for **C13-C16**. No binding was observed with complexes **C2a** and **C2b**. An increase in the fluorescence was observed for ligand **L<sub>8</sub>** and complex **C8** due to tryptamine part of ligand which leads to enhancement of fluorescence in both. These results clearly suggests that all complexes interact with both Tyr and Trp residues.

---

## 6.4 Cytotoxicity on Human Hepatoma (HepG2) cell line (*In-cellulo* assay)

*In-cellulo* assay also comes under *in-vitro* assay with only one basic difference that these studies are carried out within a cellular environment. Cell-based assays are often used to test the molecules for screening of compounds having effects on cell proliferation or show direct cytotoxic effects that eventually lead to cell death. Regardless of the type of cell-based assays used, it is important to know how many viable cells are remaining at the end of the experiments. There are a variety of assay methods exploiting different cellular properties for different targets. Basically, we have focused on enzymatic property by MTT assay.

### 6.4.1 Concept and Principle of MTT assay

This is a colorimetric assay that measures the reduction of yellow 3-(4,5-dimethylthiazol-2-yl)-2,5-diphenyl tetrazolium bromide (MTT) into an insoluble, coloured (dark purple) formazan product within the cell (**Figure 6.4.1.1**). The cells are then solubilized with an organic solvent (e.g. DMSO) and the released, solubilized formazan reagent with an absorbance maximum near 570 nm is measured spectrophotometrically. Since reduction of MTT can only occur in metabolically active cells the level of activity is a measure of the viability of the cells. Viable cells with active metabolism convert MTT into formazan product but when cells die, they lose the ability to convert MTT into formazan, thus color formation serves as a useful and convenient marker of only the viable cells. The exact cellular mechanism of MTT reduction into formazan is not well understood. Speculation in the early literature involving specific mitochondrial enzymes has led to the assumption that MTT is measuring mitochondrial activity, the reduction being caused by mitochondrial succinate dehydrogenase, but most likely involves reaction with NADH or similar reducing molecules that transfer electrons to MTT.<sup>43,44</sup>

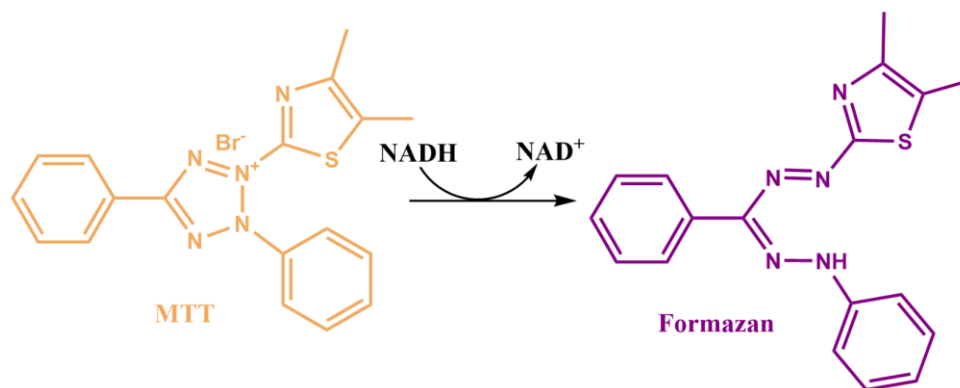


*Figure 6.4.1.1 Structure of MTT and colored formazan product.*

#### **6.4.2 Materials and instrumentation**

Human Hepatoma (HepG2) cells were procured from National Centre for Cell Science (NCCS, Pune, India). The cell lines were cultured in Dulbecco's Modified Eagle Medium (DMEM), while Phosphate Buffer Saline (PBS) was used for washing purposes. The stock solutions of compounds (1 mg/ml) were prepared by first dissolving in minimum volume of DMSO (50 $\mu$ l) and then diluting the concentrated DMSO solution with DMEM media to 1 ml. Further dilutions from the stock solution were made using DMEM for subsequent dosing. Both DMEM and PBS were purchased from Hi-Media. The MTT dye was purchased from SRL (Sisco research laboratory, Mumbai, India.). DMSO used to prepare stock solution as well as to dissolve formazan crystals was of analytical grade and purchased from Merck. 96-well culture plates were purchased from Tarson India Pvt. Ltd. The spectrophotometric detection of culture plates was done by Synergy HTX Multimode Reader. The data obtained were converted into percentage viability and were analyzed and plotted with the help of the software Graphpad Prism 3 using one-way ANOVA as the statistical tool.

#### **6.4.2 Experimental section**

The MTT reduction assay was the first homogeneous cell viability assay developed for a 96-well format.<sup>45</sup> The MTT tetrazolium assay technology has been widely adopted and remains popular in academic labs as evidenced by thousands of published articles.

In the present study, liver cancer cell line has been targeted for a few selected copper(II) complexes. These complexes have been checked for their cytotoxicity on Human Hepatoma (HepG2) cell line.

According to the standard assay, the cancer cells (HepG2) with a cell density of  $8.0 \times 10^3$  cells/ well were placed in 96-well culture plates (Tarson India Pvt. Ltd.) and seeded overnight at 37°C in a 5% CO<sub>2</sub> incubator. Compounds to be tested were then added to the wells to achieve a final concentration as per the doses fixed (the final dosing was fixed per compound as per the results of subsequent trials). Control wells were prepared by addition of culture medium without the compounds. Cells were cultured in T25 flasks in complete DMEM growth media, supplemented with 10% FBS and 1% antibiotic antimycotic solution. The cells were incubated in 5% CO<sub>2</sub> at 37°C temperature in CO<sub>2</sub> incubator (Thermo scientific, forma series II 3110, USA). Cell passaging was at 80% confluency using 1X TPVG (Himedia, India). For cytotoxic assessment, an MTT assay was performed. MTT assay is dependent on mitochondrial respiration and indicates a number of viable cells in the system. After 24h of seeding the plate was used for dosing of different target compounds. The target compounds were dissolved and prepared in an incomplete media with desired concentrations. Cells were incubated with the test compounds for 24h. Following 24h of dosing, media was removed carefully, without disturbing the cells and 3-(4,5-dimethylthiazol-2-yl)-2,5-diphenyltetrazolium bromide (MTT; 5mg/ml) was added. Mitochondrial succinate dehydrogenase reduces MTT to purple-coloured, water-insoluble formazan crystals. The plate was incubated in dark for 4h at 37°C. Resultant formazan crystals were dissolved in DMSO (150 µL/well) and kept for about 5 minutes till the crystals were completely dissolved. Absorbance was measured at 540 nm using Synergy HTX Multimode Reader. The IC<sub>50</sub> values were determined by plotting the percentage viability *versus* concentration (**Figure 6.4.3.1A-H**) and reading off the concentration at which 50% of cells remained viable relative to the control. Each experiment was repeated at least three times to obtain mean values.

### **6.4.3 Result and discussion**

*In-vitro* cytotoxicity tests of a few selected copper(II) complexes were performed on the human Hepatoma cancer cell line (HepG2). The cell viabilities (%) were obtained

with continuous exposure of the cells to the said compounds for 24 h. The cytotoxicity of the complexes were found to be dose dependent, that is, the cell viability decreased with increasing concentrations of the complexes (**Figure 6.4.3.1A-D**). The inhibitory concentration 50 ( $IC_{50}$ ), is defined as the concentration required to reduce the size of the cell population by 50%. The  $IC_{50}$  values of the complexes have been listed in **Table 6.4.3.1**.

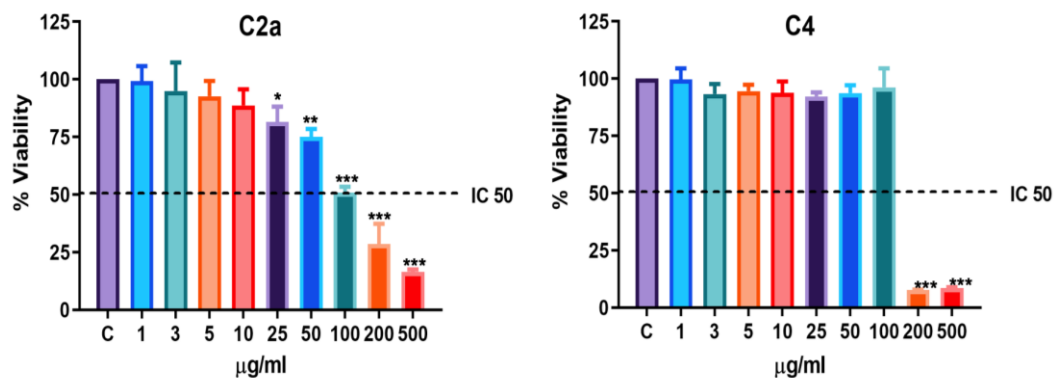


**Figure 6.4.3.1A** Cell viability verses concentration plots of (a) **C2a** (b) **C4** on human hepatoma (HepG2) cell line. Each point is the mean  $\pm$  standard error obtained from three independent experiments

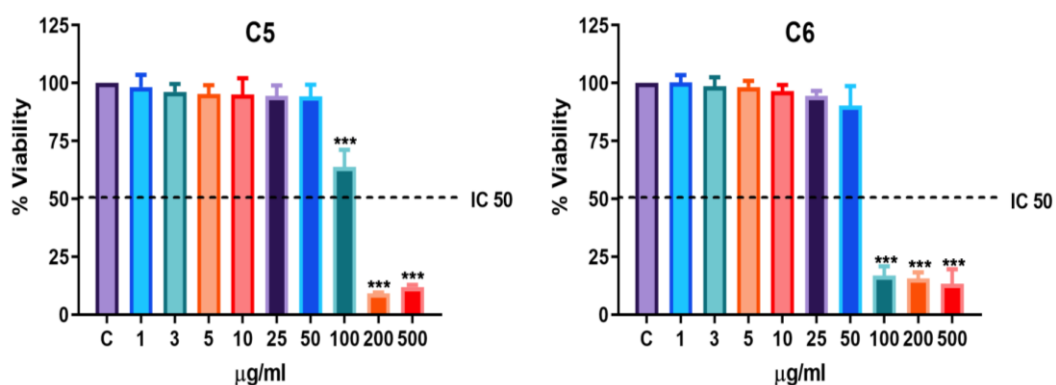


**Figure 6.4.3.1B** Cell viability verses concentration plots of (a) **C5** (b) **C6** on human hepatoma (HepG2) cell line. Each point is the mean  $\pm$  standard error obtained from three independent experiments

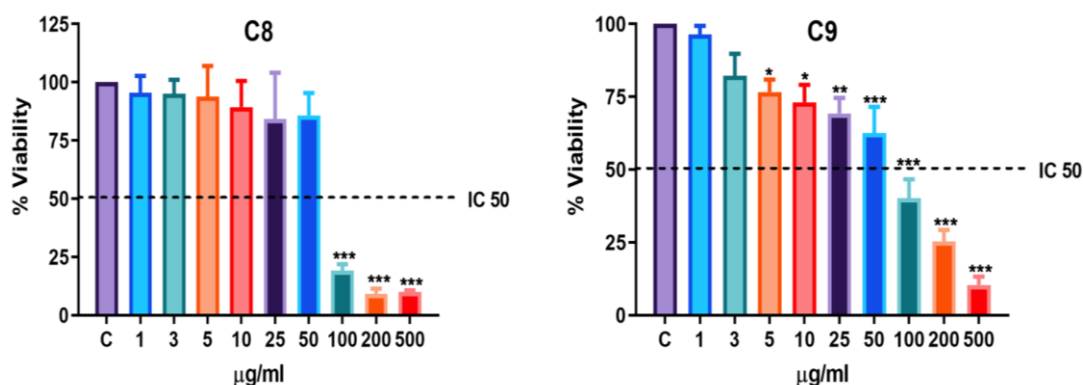


**Figure 6.4.3.1C** Cell viability versus concentration plots of (a) **C8** (b) **C9** on human hepatoma (HepG2) cell line. Each point is the mean  $\pm$  standard error obtained from three independent experiments

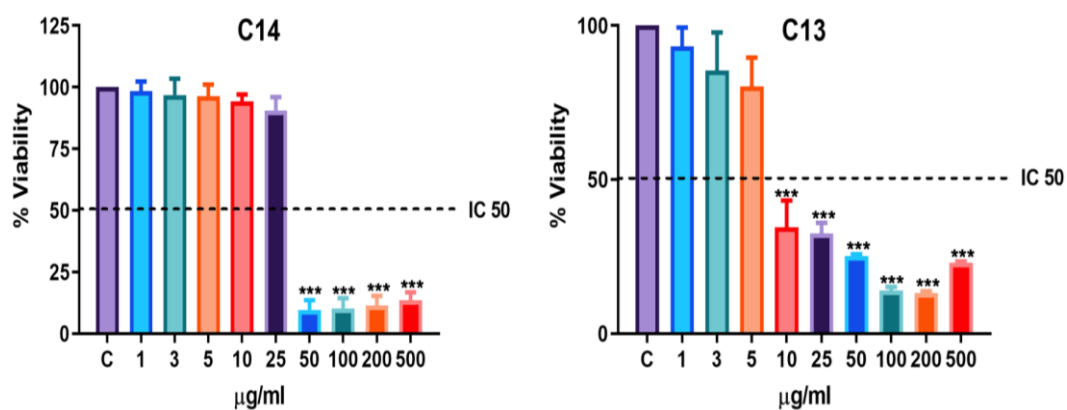


**Figure 6.4.3.1D** Cell viability versus concentration plots of (a) **C13** (b) **C14** on human hepatoma (HepG2) cell line. Each point is the mean  $\pm$  standard error obtained from three independent experiments

The *in-vitro* anticancer activity of the compounds need not be consistent with their DNA/BSA-binding abilities. The different order of biomolecular binding affinity and the *in-vitro* anticancer activity means multiple targets and multiple mechanisms coexisted in the anticancer process of the compounds. DNA/serum albumin binding need not be the only target and mechanism for cytotoxicity. Moreover, target mechanisms of the compounds may vary vividly whilst in a cellular environment.

**Table 6.4.3.1** *IC<sub>50</sub> values of complexes obtained from MTT assay on Human Hepatoma cell lines. Values have been expressed in  $\mu\text{g/mL}$ .*

Complex Codes	IC <sub>50</sub> ( $\mu\text{g/mL}$ )
<b>C2a</b>	107.3
<b>C4</b>	150.8
<b>C5</b>	103.5
<b>C6</b>	65.68
<b>C8</b>	72.28
<b>C9</b>	75.25
<b>C13</b>	8.49
<b>C14</b>	29.95
<b>Copper(II) acetate</b>	25

It was observed that complex **C13** ( $\text{IC}_{50} = <10 \mu\text{g/mL}$ ) is the most cytotoxic among all selected complexes for this activity and also when compared to its isomeric copper(II) complex **C14** ( $\text{IC}_{50} = 25\text{-}50 \mu\text{g/mL}$ ). All other complexes have cytotoxicity in the range of **50-200  $\mu\text{g/mL}$** .

## 6.5 Conclusion

All the compounds synthesized and presented in this thesis have been stepwise evaluated for their bioactivity. First the compounds have been checked for their interactions with DNA and serum albumin which are most commonly sought-after biomolecular targets for anticancer activity. DNA and BSA binding studies of synthesized complexes were studied by using UV-Vis spectroscopy and fluorescence studies. All complexes have better binding efficacies with DNA and BSA. The results so obtained prompted to go for *in-cellulo* studies. MTT assay gave an idea regarding the general cytotoxicity of the test compounds. The cytotoxicity studies reveals that complex **C13** have excellent cytotoxicity as compared to other complexes for human hepatoma (HepG2) cell line.

## REFERENCES

1. Sung, H., Ferlay, J., Siegel, R. L., Laversanne, M., Soerjomataram, I., Jemal, A. & Bray, F. Global Cancer Statistics 2020: GLOBOCAN Estimates of Incidence and Mortality Worldwide for 36 Cancers in 185 Countries. *CA. Cancer J. Clin.* **71**, 209–249 (2021).
2. Hazra, M., Dolai, T., Pandey, A., Dey, S. K. & Patra, A. Synthesis and Characterisation of Copper(II) Complexes with Tridentate NNO Functionalized Ligand: Density Function Theory Study, DNA Binding Mechanism, Optical Properties, and Biological Application. *Bioinorg. Chem. Appl.* **2014**, 104046 (2014).
3. Gomathi, R., Ramu, A. & Murugan, A. Evaluation of DNA Binding, Cleavage, and Cytotoxic Activity of Cu(II), Co(II), and Ni(II) Schiff Base Complexes of 1-Phenylindoline-2,3-dione with Isonicotinohydrazide. *Bioinorg. Chem. Appl.* **2014**, 215392 (2014).
4. Chauhan, M., Banerjee, K. & Arjmand, F. DNA Binding Studies of Novel Copper(II) Complexes Containing 1-Tryptophan as Chiral Auxiliary: In Vitro Antitumor Activity of Cu–Sn<sub>2</sub> Complex in Human Neuroblastoma Cells. *Inorg. Chem.* **46**, 3072–3082 (2007).
5. Sundaravadivel, E., Reddy, G. R., Manoj, D., Rajendran, S., Kandaswamy, M. & Janakiraman, M. DNA binding and cleavage studies of copper(II) complex containing N<sub>2</sub>O<sub>2</sub> Schiff base ligand. *Inorganica Chim. Acta* **482**, 170–178 (2018).
6. Borowska, J., Sierant, M., Sochacka, E., Sanna, D. & Lodyga-Chruscinska, E. DNA binding and cleavage studies of copper(II) complexes with 2'-deoxyadenosine modified histidine moiety. *J. Biol. Inorg. Chem. JBIC a Publ. Soc. Biol. Inorg. Chem.* **20**, 989–1004 (2015).
7. Singh, N., Pagariya, D., Jain, S., Naik, S. & Kishore, N. Interaction of copper (II) complexes by bovine serum albumin: spectroscopic and calorimetric insights. *J. Biomol. Struct. Dyn.* **36**, 2449–2462 (2018).
8. Martins, N. M. R., Anbu, S., Mahmudov, K. T., Ravishankaran, R., Guedes da Silva, M. F. C., Martins, L. M. D. R. S., Karande, A. A. & Pombeiro, A. J. L. DNA and BSA binding and cytotoxic properties of copper(ii) and iron(iii) complexes with arylhydrazone of ethyl 2-cyanoacetate or formazan ligands. *New J. Chem.* **41**, 4076–4086 (2017).
9. Pathaw, L., Khamrang, T., Kathiravan, A. & Velusamy, M. Synthesis, crystal structure, bovine serum albumin binding studies of 1,2,4-triazine based copper(I) complexes. *J. Mol. Struct.* **1207**, 127821 (2020).
10. Sharma, D., Revanasiddappa, H. D. & Jayalakshmi, B. DNA binding, BSA interaction and in-vitro antimicrobial studies of Cu(II), Co(III), Ni(II) and VO(IV) complexes with a new Schiff base. *Egypt. J. Basic Appl. Sci.* **7**, 323–341 (2020).
11. Pelosi, G., Pinelli, S. & Bisceglie, F. DNA and BSA Interaction Studies and Antileukemic Evaluation of Polyaromatic Thiosemicarbazones and Their Copper Complexes. *Compounds* **2**, 144–162, (2022).
12. Wang, Q., Mao, H., Wang, W., Zhu, H., Dai, L., Chen, Y. & Tang, X. Synthesis, X-ray crystal structure, DNA/BSA binding, DNA cleavage and cytotoxicity studies of phenanthroline based copper(II)/zinc(II) complexes. *BioMetals* **30**, 575–587 (2017).
13. Chrzanowska, A., Drzewiecka-Antonik, A., Dobrzyńska, K., Stefańska, J., Pietrzyk, P., Struga, M. & Bielenica, A. The Cytotoxic Effect of Copper (II) Complexes with Halogenated 1,3-Disubstituted Arylthioureas on Cancer and Bacterial Cells. *Int. J.*

- Mol. Sci.* **22**, (2021).
14. Mukherjee, D., Reja, S., Sarkar, K., Fayaz, T. K. S., Kumar, P., Kejriwal, A., Das, P., Sanphui, P. & Kumar Das, R. In vitro cytotoxicity activity of copper complexes of imine and amine ligands: A combined experimental and computational study. *Inorg. Chem. Commun.* **146**, 110190 (2022).
  15. Vančo, J., Trávníček, Z., Hošek, J., Malina, T. & Dvořák, Z. Copper(II) Complexes Containing Natural Flavonoid Pomiferin Show Considerable In Vitro Cytotoxicity and Anti-inflammatory Effects. *Int. J. Mol. Sci.* **22**, (2021).
  16. Ali, A., Banerjee, S., Kamaal, S., Usman, M., Das, N., Afzal, M., Alarifi, A., Sepay, N., Roy, P. & Ahmad, M. Ligand substituent effect on the cytotoxicity activity of two new copper(ii) complexes bearing 8-hydroxyquinoline derivatives: validated by MTT assay and apoptosis in MCF-7 cancer cell line (human breast cancer). *RSC Adv.* **11**, 14362–14373 (2021).
  17. Krasnovskaya, O., Naumov, A., Guk, D., Gorelkin, P., Erofeev, A., Beloglazkina, E. & Majouga, A. Copper Coordination Compounds as Biologically Active Agents. *International Journal of Molecular Sciences* **21**, (2020).
  18. Dimitrakopoulou, A., Dendrinou-Samara, C., Pantazaki, A. A., Alexiou, M., Nordlander, E. & Kessissoglou, D. P. Synthesis, structure and interactions with DNA of novel tetranuclear, [Mn<sub>4</sub>(II/II/II/IV)] mixed valence complexes. *J. Inorg. Biochem.* **102**, 618–628 (2008).
  19. Tabassum, S., Al-Asbahy, W. M., Afzal, M., shamsi, M. & Arjmand, F. DNA binding and cleavage studies of new sulfasalazine-derived dipeptide Zn(II) complex: Validation for specific recognition with 5'-TMP. *J. Lumin.* **132**, 3058–3065 (2012).
  20. Christidou, A., Zavalani, K., Hatzidimitriou, A. G. & Psomas, G. Copper(II) complexes with 3,5-dihalogeno-salicylaldehydes: Synthesis, structure and interaction with DNA and albumins. *J. Inorg. Biochem.* **238**, 112049 (2023).
  21. Tang, S.-L., Li, D.-J., Ma, F.-J., Zhang, L.-L., Lian, B., Cheng, Y.-Z. & Zhang, L.-P. Synthesis, structure, and biological properties of Cu(II) complexes based on diimine ligands. *J. Mol. Struct.* **1272**, 134229 (2023).
  22. Duckett, D. R., Murchie, A. I., Clegg, R. M., Bassi, G. S., Giraud-Panis, M. J. & Lilley, D. M. Nucleic acid structure and recognition. *Biophys. Chem.* **68**, 53–62 (1997).
  23. Marmur, J. A procedure for the isolation of deoxyribonucleic acid from microorganisms. *J. Mol. Biol.* **3**, 208-IN1 (1961).
  24. Reichmann, M. E., Rice, S. A., Thomas, C. A. & Doty, P. A Further Examination of the Molecular Weight and Size of Desoxypentose Nucleic Acid. *J. Am. Chem. Soc.* **76**, 3047–3053 (1954).
  25. Son, G. S., Yeo, J.-A., Kim, M.-S., Kim, S. K., Holmén, A., Åkerman, B. & Nordén, B. Binding Mode of Norfloxacin to Calf Thymus DNA. *J. Am. Chem. Soc.* **120**, 6451–6457 (1998).
  26. Xiao, Y.-N. & Zhan, C.-X. Studies on the interaction of DNA and water-soluble polymeric Schiff base–nickel complexes. *J. Appl. Polym. Sci.* **84**, 887–893 (2002).
  27. Pyle, A. M., Rehmann, J. P., Meshoyrer, R., Kumar, C. V., Turro, N. J. & Barton, J. K. Mixed-ligand complexes of ruthenium(II): factors governing binding to DNA. *J. Am. Chem. Soc.* **111**, 3051–3058 (1989).
  28. Zhao, G., Lin, H., Ping, Y., Sun, H., Zhu, S., Xuncheng, S. & Chen, Y. Ethylenediamine-palladium(II) complexes with pyridine and its derivatives: synthesis, molecular structure and initial antitumor studies. *J. Inorg. Biochem.* **73**,

- 145–149 (1999).
29. Dhar, S., Nethaji, M. & Chakravarty, A. R. Effect of charge transfer bands on the photo-induced DNA cleavage activity of [1-(2-thiazolylazo)-2-naphtholato]copper(II) complexes. *J. Inorg. Biochem.* **99**, 805–812 (2005).
  30. Pasternack, R. F., Caccam, M., Keogh, B., Stephenson, T. A., Williams, A. P. & Gibbs, E. J. Long-range fluorescence quenching of ethidium ion by cationic porphyrins in the presence of DNA. *J. Am. Chem. Soc.* **113**, 6835–6840 (1991).
  31. Boger, D. L., Fink, B. E., Brunette, S. R., Tse, W. C. & Hedrick, M. P. A Simple, High-Resolution Method for Establishing DNA Binding Affinity and Sequence Selectivity. *J. Am. Chem. Soc.* **123**, 5878–5891 (2001).
  32. Baguley, B. C. & Falkenhaus, E.-M. The interaction of ethidium with synthetic double-stranded polynucleotides at low ionic strength. *Nucleic Acids Res.* **5**, 161–171 (1978).
  33. Lakowicz, J. R. & Weber, G. Quenching of fluorescence by oxygen. A probe for structural fluctuations in macromolecules. *Biochemistry* **12**, 4161–4170 (1973).
  34. Zhao, D., Zhao, X., Zu, Y., Li, J., Zhang, Y., Jiang, R. & Zhang, Z. Preparation, characterization, and in vitro targeted delivery of folate-decorated paclitaxel-loaded bovine serum albumin nanoparticles. *Int. J. Nanomedicine* **5**, 669–677 (2010).
  35. He, X. M. & Carter, D. C. Atomic structure and chemistry of human serum albumin. *Nature* **358**, 209–215 (1992).
  36. Hassan, M., Azzazy, E. A. & Christenson, R. H. All About Albumin: Biochemistry, Genetics, and Medical Applications. Theodore Peters, Jr. San Diego, CA: Academic Press, 1996, 432 pp, \$85.00. ISBN 0-12-552110-3. *Clin. Chem.* **43**, (1997).
  37. Yamasaki, K., Maruyama, T., Kragh-Hansen, U. & Otagiri, M. Characterization of site I on human serum albumin: concept about the structure of a drug binding site. *Biochim. Biophys. Acta - Protein Struct. Mol. Enzymol.* **1295**, 147–157 (1996).
  38. Evans, T. W. Review article: albumin as a drug--biological effects of albumin unrelated to oncotic pressure. *Aliment. Pharmacol. Ther.* **16 Suppl 5**, 6–11 (2002).
  39. Kragh-Hansen, U. Molecular aspects of ligand binding to serum albumin. *Pharmacol. Rev.* **33**, 17–53 (1981).
  40. Lakowicz, J. R. *Principles of Fluorescence Spectroscopy 3rd Edition Springer Science+Business Media, LLC.* (2006).
  41. Temming, K., Meyer, D. L., Zabinski, R., Dijkers, E. C. F., Poelstra, K., Molema, G. & Kok, R. J. Evaluation of RGD-targeted albumin carriers for specific delivery of auristatin E to tumor blood vessels. *Bioconjug. Chem.* **17**, 1385–1394 (2006).
  42. Temming, K., Meyer, D. L., Zabinski, R., Senter, P. D., Poelstra, K., Molema, G. & Kok, R. J. Improved efficacy of alphavbeta3-targeted albumin conjugates by conjugation of a novel auristatin derivative. *Mol. Pharm.* **4**, 686–694 (2007).
  43. Marshall, N. J., Goodwin, C. J. & Holt, S. J. A critical assessment of the use of microculture tetrazolium assays to measure cell growth and function. *Growth Regul.* **5**, 69–84 (1995).
  44. Berridge, M. V & Tan, A. S. Characterization of the cellular reduction of 3-(4,5-dimethylthiazol-2-yl)-2,5-diphenyltetrazolium bromide (MTT): subcellular localization, substrate dependence, and involvement of mitochondrial electron transport in MTT reduction. *Arch. Biochem. Biophys.* **303**, 474–482 (1993).
  45. Mosmann, T. Rapid colorimetric assay for cellular growth and survival: application to proliferation and cytotoxicity assays. *J. Immunol. Methods* **65**, 55–63 (1983).